Reservoir fluids and their migration into the South Eugene Island Block 330 reservoirs, offshore Louisiana

Steven Losh, Lynn Walter, Peter Meulbroek, Anna Martini, Lawrence Cathles, and Jean Whelan

ABSTRACT

This study in the well-documented Pliocene–Pleistocene South Eugene Island Block 330 (SEI330) field, offshore Louisiana, unravels a complex petroleum system by evaluating both the inorganic and organic geochemical characteristics of reservoir fluids. The brines at SEI330 dissolved halite prior to entering the reservoirs and equilibrated with reservoir sediments, exchanging sodium for calcium, magnesium, and other cations. The systematically varying extent of brine sodium depletion in two reservoirs defines south to north flow in those sands. These sands were filled from a fault that bounds the reservoirs on the south. Oil compositional parameters also show north-south variation across these reservoirs. The SEI330 oils and gases each had different sources. In contrast to published Jurassic sources for oil, carbon isotope data indicate that SEI330 hydrocarbon gases probably sourced from early Tertiary or Cretaceous sediments, after oil had migrated through them. Distribution of biodegraded vs. unbiodegraded oils indicates the reservoirs filled much more recently than formation of the salt weld beneath the field. Oil compositions indicate that some SEI330 oils were partially stripped of low–molecular weight compounds by their dissolution in a mobile vapor phase (gas washed) by large volumes of gas several hundred meters below the deepest reservoir. Modeling of this gas-oil interaction aids in identifying deep potential targets in which gas washing occurred.

Hydrocarbon distribution, combined with oil chemistry and reservoir pressures, indicate reservoirs filled from fault systems on both the north and south sides of the field. The fault feeders are wide (>100 m), structurally complex zones that can direct different types of fluids into different reservoirs.

Manuscript received September 2, 1999; revised manuscript received January 10, 2001; final acceptance January 24, 2002.

AUTHORS

STEVEN LOSH ~ *Department of Geological Sciences, Snee Hall, Cornell University, Ithaca, New York, 14853; losh@geology.cornell.edu*

Steven Losh earned a B.S. degree with high honors in geological engineering at the Colorado School of Mines and a Ph.D. in geology at Yale University. His work focuses on the integration of geochemical and geological data to address problems of fluid flow in a variety of settings.

LYNN WALTER ~ *University of Michigan, Department of Geological Sciences, 2534 C. C. Little Building, 425 E. University Avenue, Ann Arbor, Michigan, 48109; lmwalter@l.imap.itd.umich.edu*

Lynn M. Walter received her M.S. degree from Louisiana State University (1978) and her Ph.D. from the University of Miami (1983). She was an assistant professor at Washington University in St. Louis until 1988. She then joined the University of Michigan, where she is now a professor of geological sciences and director of the Experimental and Analytical Geochemistry Laboratory. Her research interests focus on the hydrogeochemistry of near-surface and deeper basin environments, with an emphasis on carbon transformations and mineral mass transport.

PETER MEULBROEK ~ *Materials and Process Simulation Center, California Institute of Technology, 1600 E. California Road, Pasadena, California, 91101; meulbroek@wag.caltech.edu*

Peter Meulbroek received a B.S. degree in mathematics from the University of Chicago and a Ph.D. in geology from Cornell University. He is currently working at Caltech at the Molecular and Process Simulation Center. His interests there include modeling macroscopic chemical behavior with equations of state, microscopic behavior using molecular dynamic and quantum mechanical models, and developing data-centric models for all scales.

ANNA MARTINI ~ *Department of Geology, Campus Box 2238, Amherst College, Amherst, Massachusetts, 01002; ammartini@amherst.edu*

Anna Martini received her B.A. degree in geology from Colgate University, her M.S. degree in geology from Syracuse University, and her Ph.D. in geology from the University of Michigan. She is currently an assistant professor of geology at Amherst College. Her research to date has focused on unconventional natural gas plays in the Michigan and Illinois basins.

LAWRENCE CATHLES ~ *Department of Geological Sciences, Snee Hall, Cornell University, Ithaca, New York, 14853; cathles@geology.cornell.edu*

Lawrence Cathles received his A.B. degree and Ph.D. from Princeton University. He was employed in research by Kennecott and later by Chevron and is currently a professor of geological sciences at Cornell University. He has been involved in modeling fluid flow and chemical processes related to both ore deposits and sedimentary basins, with a major focus on three-dimensional finite element–coupled fluid flow and chemical models for petroleum systems in the Gulf of Mexico.

JEAN WHELAN ~ *Department of Marine Chemistry and Geochemistry, Fye Laboratory, Woods Hole Oceanographic Institute, Woods Hole, Massachusetts, 02543; jwhelan@whoi.edu*

Jean Whelan is a senior research specialist. She became interested in organic geochemistry through her mentor at Woods Hole, John M. Hunt. Her current research focuses on use of organic compounds as indicators of geologic and oceanographic processes, particularly with respect to gas and oil formation, migration, and destruction both in subsurface sediments and in the ocean. Her past research focused on gases and light hydrocarbons in oceanic environments and on microbial transformations in shallow and deep ocean sediments. Whelan earned her bachelor's degree in chemistry from the University of California at Davis and her doctorate in organic chemistry from the Massachusetts Institute of Technology.

ACKNOWLEDGEMENTS

Support for this work was provided by Gas Research Institute contract GRI50972603787 to L. Cathles, Cornell University, with a subcontract to J. Whelan at Woods Hole Oceanographic Institute (WHOI). Corporate sponsors of the Global Basins Research Network (GBRN) provided additional support. The analyses reported herein were obtained under U.S. Department of Energy grant DE-FC22-93BC14961 to Roger Anderson, Lamont-Doherty Earth Observatory, with subcontracts to L. Cathles, Cornell University, and J. Whelan, WHOI. We thank Pennzoil Exploration and Production Co. (now Devon Energy) and their partners for their generous cooperation in this project. S. Losh thanks Glen Wilson for helpful discussions. We also thank Bruce Hart, Roger Sassen, Jeff Hanor, and an anonymous reviewer for thoughtful and constructive formal and informal reviews of this article.

INTRODUCTION

Knowledge of fluid migration pathways and of processes that affect fluid composition is particularly important for evaluating exploration risk in complex geologic settings in which fluids have flowed long distances and have experienced interaction with gas, sediment, and other liquids along the way. Such a setting exists in the Gulf of Mexico, where the geology is dominated by the interaction among salt tectonics, faulting, and rapid deltaic and slope sedimentation. There, oil generated in Mesozoic rocks (Thompson et al., 1990), now buried at depths up to 14 km, is subject to chemical modification along its migration pathway to shallower sands that are targeted for exploration. To evaluate the nature of migration paths and understand how reservoirs filled in this setting, we have investigated reservoir fluids and their related plumbing system at the South Eugene Island Block 330 (SEI330) field, offshore Louisiana. This field, which contained initial recoverable reserves of 307 million bbl oil and 1.5 tcf gas, has been the subject of intensive study by several workers and is a natural laboratory for developing an understanding of the nature of, and controls on, fluid migration and reservoir filling. To develop this understanding, we assess the distribution of fluids within the various reservoirs. Are fluids essentially the same within all of the reservoirs, or do they differ vertically? If they differ vertically, do the differences reflect migration from oil accumulations at different places and/or times within the petroleum system? Do the fluids show any compositional variations within reservoirs that can illuminate filling direction and so be used to constrain or distinguish the migration pathways into the reservoir? What is the timing of reservoir filling, and what are the geologic controls on fluid migration?

To address these questions, we focus on chemical description of the component species within the reservoirs: brine, oil, and gas. We specifically consider those chemical markers that distinguish fluids in one reservoir from those in another, provide information on timing of reservoir filling, or indicate direction of flow. The geologic setting of the SEI330 field, and the evolution of the Block 330 minibasin, have been described in detail by Holland et al. (1990), Rowan et al. (1994), and Alexander and Flemings (1995). Hart et al. (1997) described the stratigraphy of one of the major reservoir sands, the GA. Details of the minibasin-bounding fault system are given by Rowan et al. (1998), Alexander and Handschy (1998), Losh (1998), and Losh et al. (1999). As the geology is well described in these articles, it is only summarized in the following section.

The SEI330 oils were studied by Whelan et al. (1994), who concluded that they were sourced from early Cretaceous or Jurassic marine source rocks and that the oils are similar to one another in terms of source and maturity. Schumacher (1993) and Whelan et al. (1994) described late migration of gas condensates into biodegraded reservoirs. Meulbroek (1997) and Meulbroek et al. (1998) described gas washing of oil at Block 330. Moran et al. (1995) determined Oligocene–Jurassic ages for reservoir brines on the basis

of ^{129}I concentrations. The purpose of this article is to present new data and new interpretations of existing data bearing on fluid chemistry within the reservoirs, building on the existing geochemical work. We also integrate these data with the known geologic setting to better understand the nature of, and controls on, fluid migration and accumulation at the SEI330 field. In so doing, we demonstrate some techniques that have broader applicability in evaluating petroleum systems in terms of timing and direction of migration and in terms of gas-oil interactions that can point to deeper targets.

GEOLOGIC SETTING

The SEI330 field contains original in-place reserves of 750 million bbl oil and 2.2 tcf gas, with recoverable reserves of 307 million bbl oil and 1.5 tcf gas (Holland et al., 1990). Production is from fault traps and four-way closures in two anticlines, primarily on the downthrown side of a large growth-fault system, termed the A fault zone (Figure 1). Reservoirs comprise 25 different faulted unconsolidated sands that were deposited in an upward-shoaling sequence in a salt-withdrawal minibasin (Figure 2) (Holland et al., 1990; Alexander and Flemings, 1995). The 1 km–thick reservoir section in Block 330 overlies approximately 600 m of massive prodelta shale, which in turn overlies turbidite and slope fan sands and prodelta/slope facies shales (Alexander and Flemings, 1995). The alphabetically named reservoir section itself consists of fluvial and deltaic sands (GA, 0.9 Ma) overlying deltaic sands (HB–OI) (Figure 2) that range in age from 1.0 (HB) to 1.8 Ma (OI) (Alexander and Flemings, 1995).

Reservoir sands were deposited in a salt-withdrawal minibasin that developed atop a salt body that was emplaced in the early–middle Tertiary (Rowan et al., 1994). According to the palinspastic reconstructions of Rowan (1995), a salt weld began to form beneath the minibasin at approximately 1.4 Ma and was largely in place by 0.8 Ma. The tectonostratigraphic analysis of Alexander and Flemings (1995) shows that the salt weld began to form near the end of the main phase of deltaic sedimentation, between approximately 1.2 and 1.0 Ma. The timing of salt weld formation is important for understanding the controls on oil and gas migration to the Block 330 reservoirs, as such migration must have occurred after the weld opened a pathway from sub-minibasin migration routes into minibasin reservoirs.

The combined A fault–antithethic fault system controls the distribution of oil and gas within the downthrown reservoirs. Structures in Block 331, which contain sand of similar thickness and quality to that in the Block 330 reservoirs, are only charged when the correlative reservoirs in Block 330 are filled to their synclinal spillpoint into Block 331. This indicates the traps in Block 330 filled first, then spilled into Block 331 (Losh et al., 1999). Such a charging history precludes updip migration from the center of the minibasin and indicates these reservoirs filled from the complex fault system at the eastern end of the minibasin.

The main reservoir section is bounded on the north and northeast by a major growth fault (the A fault zone) that has been demonstrated to have acted as a conduit for reservoir fluids (Losh, 1998; Losh et al., 1999; also see Alexander and Handschy, 1998). To the south, the reservoir sands are bounded by an antithetic fault (Alexander and Flemings, 1995). At its eastern end in Blocks 337 and 338, this fault is interpreted on seismic data to cut nearly to the sea floor. Both the A fault in SEI330 and the antithethic fault in Block 338 have remained active, thus transmissive to fluids, at least throughout the Pleistocene (Alexander and Flemings, 1995). At the depth of the OI sand (7300 ft [2225 m]) in the A20ST well in Block 330, the A fault zone is more than 100 m wide (Losh, 1998; Losh et al., 1999). On the basis of observations of fault zone core combined with Formation MicroImager log images, the fault is known to contain several high-strain gouge zones that separate blocks of variably faulted, oil-charged sediment. Oil has been encountered in the A fault zone in several wells (Anderson et al., 1994a, b; Losh et al., 1999), and gas shows are encountered in nearly every fault cut in Block 330 (J. Austin, 1993, personal communication). Losh (1998) demonstrated that, in at least one location, fluid transmission in the fault was linked to tectonic activity of the fault and observed that structural complexities such as branch lines may localize fluid flow in these faults. The main faults are thus identified as wide, structurally complex zones that acted as feeders for the downthrown Block 330 reservoirs.

RESERVOIR BRINE CHEMISTRY

Results

Twenty-two brine samples were collected in the winter of 1994 from platforms in Blocks 330 and 316. Sample

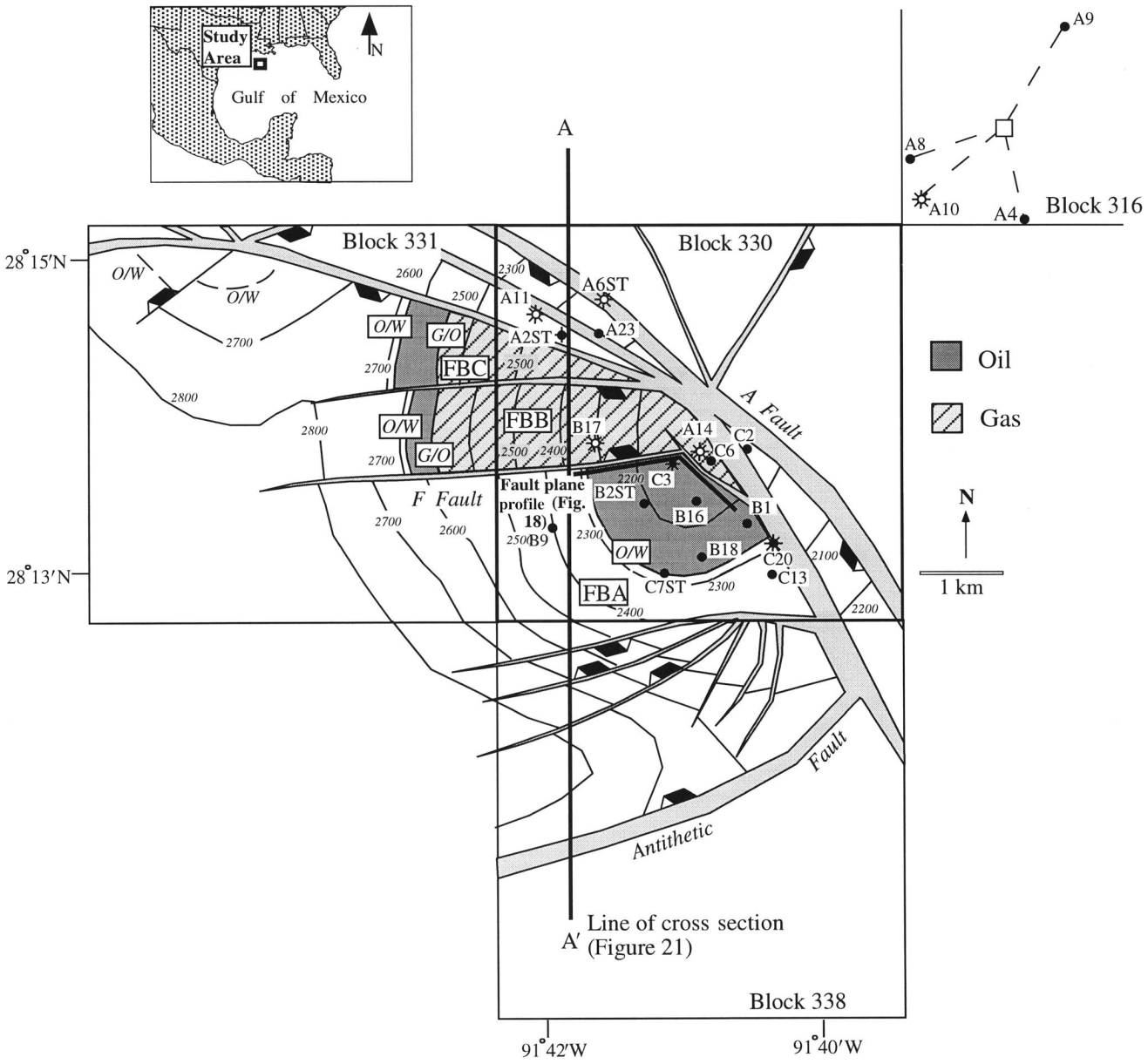

Figure 1. Location map, showing wells from which brine samples were collected. Structure contour map is on top of OI-1 sand, modified from Holland et al. (1990), with contours and fault pattern in Block 338 modified from Alexander and Flemings (1995). Contours are in meters subsea true vertical depth (TVD).

preparation and analytical procedures are given in the Appendix, and the data are presented in Table 1. The brine samples show a three-fold range in salinity, which is in part dependent on reservoir. Brines from the GA sand have nearly twice the chloride content as those from the HB sand, just 150 m lower in the section (Table 1). In contrast, mean cation and anion concentrations for magnesium, potassium, and the conservative tracer bromide show little difference from seawater values, nearly regardless of brine salinity. The lack of correlation between chloride and bromide, together with the near constancy of Block 330 Br^- concentration at values only slightly greater than seawater (67 mg/L), indicate that chloride increases are attributable to salt dissolution rather than to evaporative concentration of brine (Figure 3a). Mesozoic evaporative brines of the kind that Land and MacPherson (1989) suggested were present in Pliocene–Pleistocene sediments on the basis of elevated Br^- concentrations are not represented in the Block 330 sample set. Sodium and chloride are strongly correlated, but molar sodium is deficient relative to chlo-

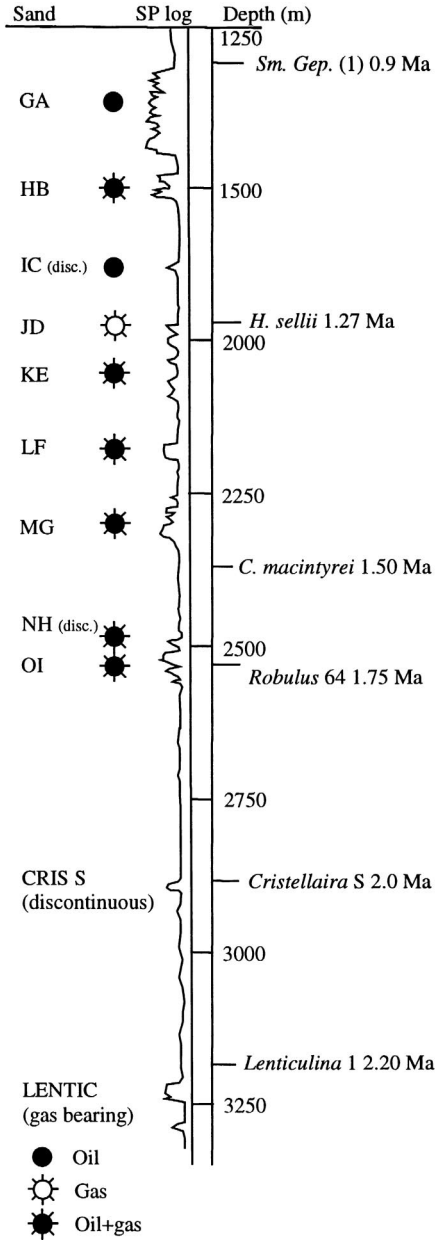

Figure 2. Composite well log, downthrown side of A fault, Block 330 (modified from Holland et al. [1990] and Alexander and Flemings [1995]). Ages and depositional environments are from Alexander and Flemings (1995).

ride in nearly every sample (sodium deficiency shown in Figure 3b).

The brines are currently in chemical equilibrium with reservoir sediments. This is shown, for example, by the linear trends of $[Ca^{2+}]/[H^+]^2$ vs. $[Na^+]/[H^+]$ for GA and HB brines (Figure 4). Potassium and silicon (not shown) have similar dependencies on pH. As pH is proportional to salinity in sediment-buffered systems, this dependence indicates sediment buffering of the brine chemistry. Furthermore, Mg-Li geothermometry (Kharaka and Mariner, 1989) of brines in the various reservoirs yields temperatures (Table 1) that are generally in agreement with measured reservoir temperatures, consistent with buffering of Mg and Li by reservoir sediments. Although in-situ albitization is absent, quartz and feldspar in the GA and HB sands are commonly pitted on the scale of microns (Losh, 1995), perhaps as a result of high brine salinity promoting dissolution as envisioned by Hanor (1996). As is described in a following section, brine chemistry probably has been significantly modified by means of reaction with reservoir sediment.

Several lines of evidence indicate that sodium deficiency in the brine (Figure 3b) is due to brine-sediment interaction. Sodium deficiency correlates with other indices of sediment-brine interaction, including $^{87}Sr/^{86}Sr$ (Figure 5a), and Sr content (Figure 5b). These two parameters were modified by brine interaction with sediments, as shown by their covariation in Figure 6. The current chemical equilibrium between brines and reservoir sediments illustrated in Figure 4 indicates that brine-sediment interaction has occurred within the reservoirs. Some, if not all, of the sodium loss and Sr (and other cation) gain may have resulted from brine interaction with reservoir sediments. The extent of sodium deficiency is correlated with the concentration of several cations, including calcium (Figure 7a), potassium, magnesium, strontium (Figure 5b), and barium, suggesting that these cations have been liberated from sediment by exchange with sodium. As shown in Figure 7b, the sum of the charges of the exchanged cations in the brines is approximately equal to the sodium deficiency as defined in Figure 3b, consistent with cation exchange and possible mineralogical reactions predominantly involving clays.

Brine ^{129}I concentrations and strontium isotopic compositions indicate substantial vertical migration of fluid into the Block 330 sands. The least radiogenic value, 0.70804, is compatible with seawater of at least Oligocene age (i.e., Hoefs, 1981). Salinity and ^{129}I ages (reported by Moran et al. [1995]) define distinct brines in the GA, HB, and OI sands (Figure 8). The similarity in ^{129}I ages between the HB and the younger GA brines suggests a common source for those brines, whose different salinities indicate variable amounts of salt dissolution. The older GA brines clearly had a different source from the HB brines. As shown by their $^{87}Sr/^{86}Sr$ ratios and Sr concentrations (Figure 6), both older and younger GA brines have interacted to a greater extent with clastic sediments along their flow

Table 1. Brine Chemical Data and Selected Chemical Parameters*

Sand	Well	TVD (m)	TC	pH	ρ (g/ml)	Na	Ca	Mg	Sr	CO_2	K	Si	Cl	SO_4	Br	Zn	Li	AlkT	Charge Balance	87/86	I**	I-age**	$\delta^{18}O$	$\delta^{13}C$	Na Deficiency	Acetate	Propanoate	TMg-Li†	Res TC	TNaKCa†
Block 330																														
GA-2	B1D	1284	33	6.79	1.108	56200	3260	1350	186	2.9	255	10.7	97100	<3	81	1.1	1.72	4.99	−0.3	–	42	58	–	–	−203	275	<10	51	50	33
GA-2	B16D	1289	34.4	7.07	1.103	52200	3170	1490	170	5.2	237	10.9	92500	<3	88	0.7	1.49	5.92	−1.1	–	40	31	–	–	−248	<50	<10	47	50	27
GA-2	B18D	1297	30	7.05	1.11	57200	3550	1700	197	3.2	303	11	98600	<3	84	0.4	2.32	4.11	0.6	–	39	59	–	–	−203	65	<10	54	50	27
GA-2	C2D	1292	43.2	6.9	1.093	47100	2880	1420	159	7	273	15.6	79200	<3	87	0.6	2	10.45	1.6	0.70855	36	53	0.11	11.74	−95	<50	<10	53	50	26
GA-2	C6D	1282	–	6.9	1.112	56400	3320	1390	199	3.4	288	14.5	103000	<3	82	0.6	2.35	5.27	−2.9	–	–	–	–	–	−361	<50	<10	57	50	33
GA-2	C7ST	1297	28	6.91	1.104	51800	3050	1560	163	9	255	16.4	91200	<3	87	0.4	1.82	13.39	−0.9	–	36	40	–	–	−228	120	<10	50	50	24
GA-2	C13D	1288	40	7.04	1.113	58200	3330	1350	198	4.3	295	11.1	103100	<3	83	0.7	2.78	4.86	−1.6	0.70875	36	35	0.68	8.42	−285	<50	<10	61	50	35
GA-2	C20	1283	24	6.91	1.109	54000	3150	1500	182	3.9	271	14.3	96600	<3	88	0.5	2.1	6.32	−1.7	–	35	58	–	–	−285	176	<10	54	50	27
HB-1	B2ST	1453	33	7.12	1.058	32800	2020	1310	94.1	4.9	242	12.8	55800	<3	79	0.4	2.24	6.41	1.9	–	44	42	–	–	−58	135	<10	56	54	17
HB-1	B17D	1470	34.4	7.15	1.067	31200	2030	1360	73.1	6.5	186	12.8	54600	<3	80	0.4	1.19	7.52	0.9	0.70821	40	37	−0.44	2.38	−94	<50	<10	43	54	15
HB-1	C2	1457	47	6.81	1.068	31200	2110	1330	85	9.6	251	17.9	56000	<3	80	0.5	2.21	10.52	−0.3	–	37	37	–	–	−133	<50	<10	56	54	18
HB-1	C3D	1449	–	7.05	1.073	32200	2310	1490	108	4.9	276	13.5	60900	<3	79	0.5	1.74	5.39	−2.3	0.70820	40	38	−0.72	11.23	−227	<50	<10	50	54	17
JD	A11	1948	38.2	6.93	1.076	33400	3920	1680	150	3.8	251	14.3	63400	<3	66	0.6	2.24	8.26	0	–	40	39	–	–	−245	2400	820	54	62	31
KE	A6ST	1927	–	6.91	1.092	43400	4130	1820	142	4	373	30.5	80800	<3	103	0.6	8.38	6.06	−0.7	–	47	31	–	–	−301	1220	501	83	64	31
MG-3	B9	2257	25.6	6.47	1.085	38600	4000	1660	161	2.1	300	47.5	73700	–	81	0.5	2.17	8.47	−1.5	–	41	51	–	–	−310	5280	685	53	68	33
OI-1	A14A	2154	35.1	6.97	1.101	51600	2940	813	227	4	240	24.2	90000	<3	76	0.6	3.12	9.11	−1.6	0.70833	46	46	1.76	1.36	−203	3990	1000	69	70	55
OI-4	A23	2145	–	7.03	1.076	33200	3460	1050	142	3.7	251	17.5	64000	<3	110	3	4.19	13.86	−3	–	42	54	–	–	−271	2490	627	73	72	48
OI-5	A2ST	2243	39.4	7.03	1.042	19900	1550	506	43.8	5.3	122	29.7	33100	–	99	0.3	4.82	30.6	1.2	0.70804	48	48	−0.2	−2.63	21	13600	2200	85	72	44
Block 316																														
MG	A9	2134	38.4	6.77	1.109	48800	2260	863	147	4.8	471	19	80200	<3	45	1	7.42	4.95	1.1	–	–	–	–	–	−49	<50	<10	90	–	48
L-1	A4	2342	37.8	6.82	1.104	51900	3270	1530	174	3.4	344	32.7	90800	<3	417	25.1	2.76	4.97	−0.2	–	–	–	–	–	−213	–	–	59	–	30
L-1	A8A	2353	–	6.46	1.105	54100	2640	1280	153	3.8	303	14.3	94100	<3	314	23.6	3.71	11.47	−1.3	–	–	–	–	–	−210	–	–	68	–	29
L-1	A10	2325	–	–	1.097	48700	3380	1540	128	2.7	309	18.9	85400	<3	463	19.7	4.13	7.39	0.1	–	–	–	–	–	−200	–	–	68	–	30
Seawater					1.024	10770	412	1290	8	–	380	2	19400	905	67	.005	.18	–	–	–	0.06	–	–	–	–	–	–	–	–	–

*Except where noted, data were generated at University of Michigan. Cations and anions in mg/L, except CO_2, which is in mM, and AlkT, which is in mequiv/L; $\delta^{18}O$ and $\delta^{13}C$ in PDB scale; Na deficiency in mM; acetate and propanoate in μM.

**Data from Moran et al., 1995.

†Temperatures calculated according to Kharaka and Mariner (1989).

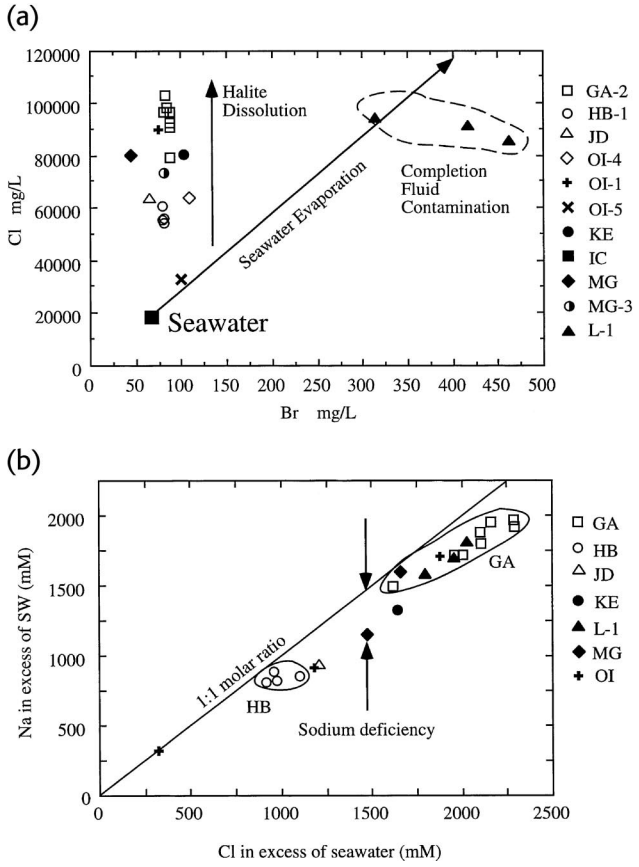

Figure 3. (a) Chloride vs. bromide, Block 330 brines. Seawater evaporation and halite dissolution trends are shown. Three samples that have elevated Br content also show high Zn content (Block 316 L-1 samples in Table 1), reflecting contamination by $ZnBr_2$ completion fluid. These wells were completed within two years of sampling. (b) Plot of sodium (mM) in excess of seawater concentration vs. chloride (mM) in excess of seawater concentration. Line shows 1:1 molar ratio, expected for halite dissolution. Most brines show depletion of Na relative to Cl, indicating interaction of brine with sediment. The deviation in excess Na from a 1:1 molar ratio with excess Cl is herein referred to as "sodium deficiency."

path than either the HB or the OI brines. Several brine types can be discerned from the chemical data (Figure 8). First, relatively young (30–40 Ma) brine followed different paths to the GA and HB reservoirs, with the GA brine dissolving more salt than the HB brine. Next, relatively old (40–55 Ma) saline brine is present in the GA reservoir but not in the HB. Finally, a variety of old (40–54 Ma) brines filled the OI and other sands, having a wide range of salinity and extent of interaction with clastic sediment. These different sources and flow paths indicate brine migration through a complex, and probably temporally variable, plumbing system.

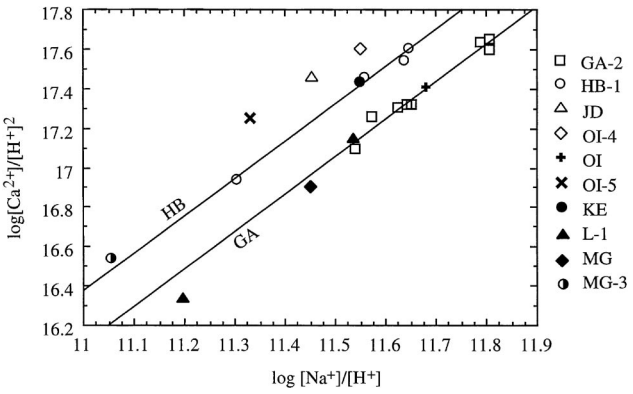

Figure 4. Diagram of $[Ca^{2+}]/[H^+]^2$ vs. $[Na^+]/[H^+]$ showing straight line best fits ($r^2 > 0.98$) for the GA and HB brines. The brines are in chemical equilibrium with reservoir sediments, in particular with clays.

Discussion of Brine Chemistry

Reservoir brine chemistry illustrates the effects of brine-sediment interaction, which can be interpreted in terms of the nature and direction of fluid flow to and within the reservoirs. The high chloride and high iodide concentrations (Table 1) preclude mixing of reservoir brines with any significant quantity of seawater or meteoric water from the surface since the reservoirs were filled, because these would have diluted the reservoir fluids. The iodine concentrations in Block 330 brines are, with the minor exception of some onshore locations, among the highest that have been observed in clastic sediments in the Gulf of Mexico (MacPherson, 1989; Moran et al., 1995) and are nearly three orders of magnitude higher than seawater, so significant dilution is unlikely. Small fractions of residual pore fluids (connate fluid) could have mixed with deeply sourced brine in the GA and HB reservoirs. In these reservoirs, brine iodide content decreases in a northerly direction (see Figure 9). The pattern of iodine concentration in the GA sand is similar to that observed for brine salinity derived from spontaneous potential (SP) logs by Lin and Nunn (1997). If mixing between deep brine (high I^-) and connate water initially in the pore space (low I^-) accounts for the observed variation in iodine concentration, the fraction of residual seawater in the mixed fluid increases to the north. This implies that deeply sourced, high-iodine brines migrated from south to north in these sands.

Insofar as sediments take up sodium from the brine, sodium deficiency may be used as an indicator of flow direction. In particular, brine sodium deficiency

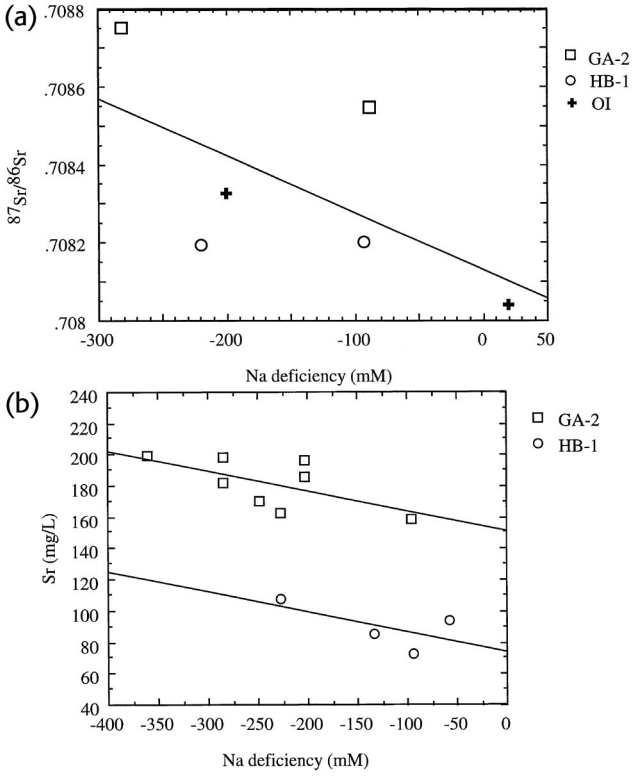

Figure 5. (a) Sodium deficiency vs. brine $^{87}Sr/^{86}Sr$. Increasing water-sediment interaction results in greater brine sodium deficiency. Scatter may result from different mechanisms being responsible for modification of brine $^{87}Sr/^{86}Sr$ (carbonate recrystallization, as well as cation exchange involving clays) as opposed to uptake of sodium, which is affected solely by cation exchange. (b) Brine Sr vs. sodium deficiency. The Sr increases as sodium is consumed from brine; both track brine-sediment interaction.

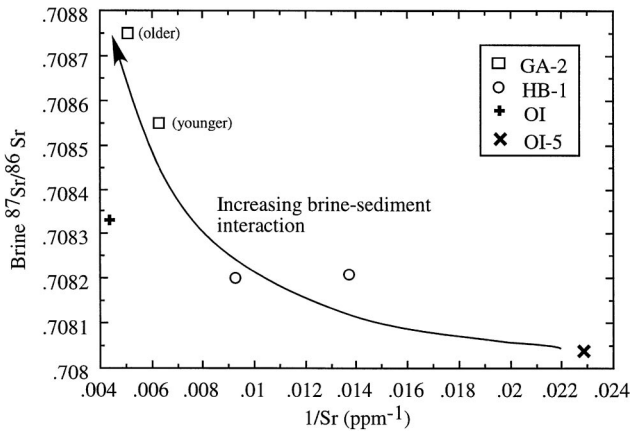

Figure 6. Brine $^{87}Sr/^{86}Sr$ vs. 1/Sr. Brine Sr isotopic composition tracks the extent of water-sediment interaction. Older GA brine has an ^{129}I age of 53 Ma; younger GA brine has an ^{129}I age of 35 Ma (Table 1).

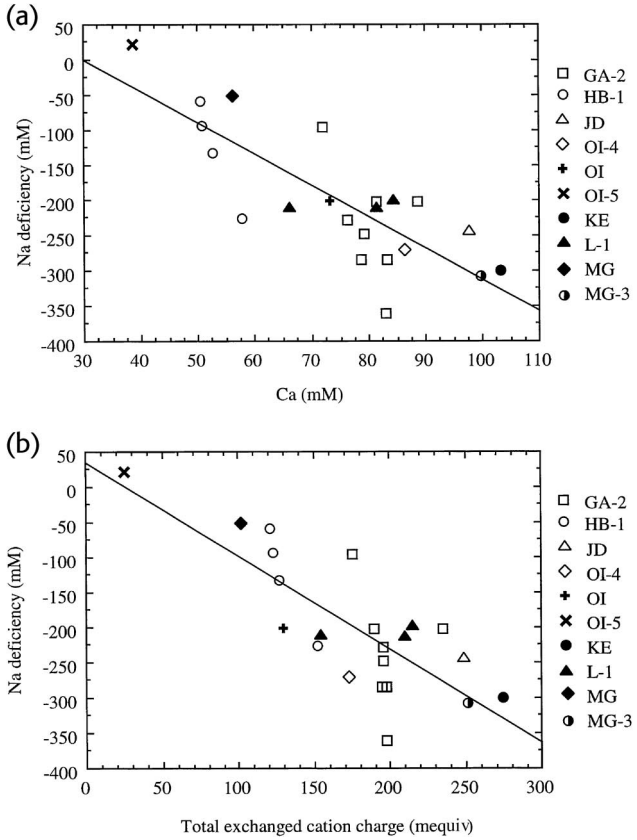

Figure 7. (a) Brine sodium deficiency vs. Ca concentration. Preexchange Ca^{2+} concentration in the brine is interpreted as that which corresponds to zero sodium deficiency and is about 40 mM. (b) Brine sodium deficiency (mM) vs. total milliequivalents of charge from cations that exchanged with sodium, computed from present concentrations minus preexchange concentrations as determined in caption to Figure 7a. This total includes all cations that correlate with Na deficiency: Ca^{2+}, Mg^{2+}, K^{+}, Sr^{2+}, and Ba^{2+}. The charge from exchanged cations is computed in mequiv as $2(([Ca^{2+}] - 40) + ([Mg^{2+}] - 20) + ([Sr^{2+}] - 0.8) + ([Ba^{2+}] - 0.3)) + ([K^{+}] - 3.0)$, where all concentrations are in mM. The expected slope for simple cation exchange is -1.0; the actual slope is -1.2.

would be expected to increase along the flow path of a particular volume of brine, tracking the extent of brine-sediment interaction. Contours of sodium deficiency for GA and HB brines, the best-sampled reservoirs, show increasing sodium deficiency from south to north (Figure 10). If the length of the flow path through sediment (that is, the amount of brine-sediment contact) is the dominant control on sodium deficiency, the map patterns indicate the brines flowed from the south to southwest in these sands. Such a flow direction is compatible with that suggested by the iodine distribution shown in Figure 9, which implies in-

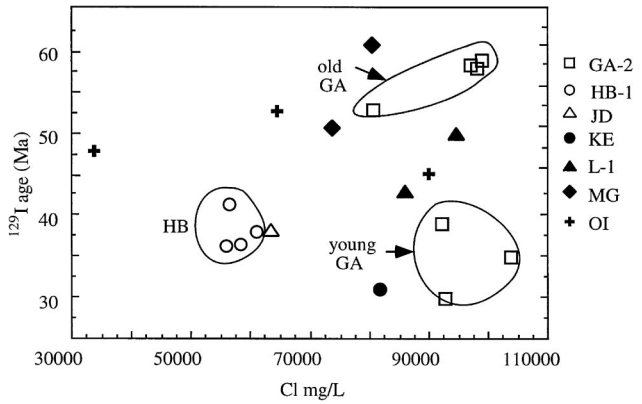

Figure 8. Brine ^{129}I age vs. Cl concentration (mg/L) for each reservoir. The GA brines are highly saline and have two distinct age groupings: 30–40 Ma and 52–62 Ma. The HB brines have ages of 37–42 Ma, indicating that older GA brines have a different source than do the HB brines and that younger GA and HB brines had different histories relative to interaction with salt.

creasing fractions of original pore fluid (seawater) mixed with the deeply sourced brines in the northern and northeastern parts of these reservoirs. The lone exception to this pattern, the C2 sample (sodium deficiency of 95 mM, in the GA sand) at the northeast extreme of the sample set, may reflect mixing of brine with fluid that migrated from a different direction or originated below the nearby oil-water contact.

The regular spatial variation of sodium deficiency across the GA and HB reservoirs (Figure 10) indicates that much if not all of the brine sodium deficiency may be due to interaction with sediments within the reservoirs themselves. Except for the low value (95 mg/L) in the C2 well in the northeastern part of the GA reservoir, the spatial variation in sodium deficiency in that reservoir is not related to height above, or lateral distance from, the oil-water contact. Thus, the spatial pattern of sodium deficiency represents in-situ brine chemical variations rather than mixing between brines in the oil leg and those in the water leg in the GA sand. The correlation between sodium deficiency, which in large part reflects brine-sediment interaction within the reservoirs, and brine $^{87}Sr/^{86}Sr$ indicates that much of the ^{87}Sr enrichment of the brine also occurred within the reservoir. This positive correlation suggests that the brines all had relatively low $^{87}Sr/^{86}Sr$ values prior to entering the reservoirs, which in turn implies that little brine-sediment interaction occurred as the brines ascended from their source to the reservoirs. The low extent of brine-sediment interaction is consistent with the ascent of brine primarily through a fault/

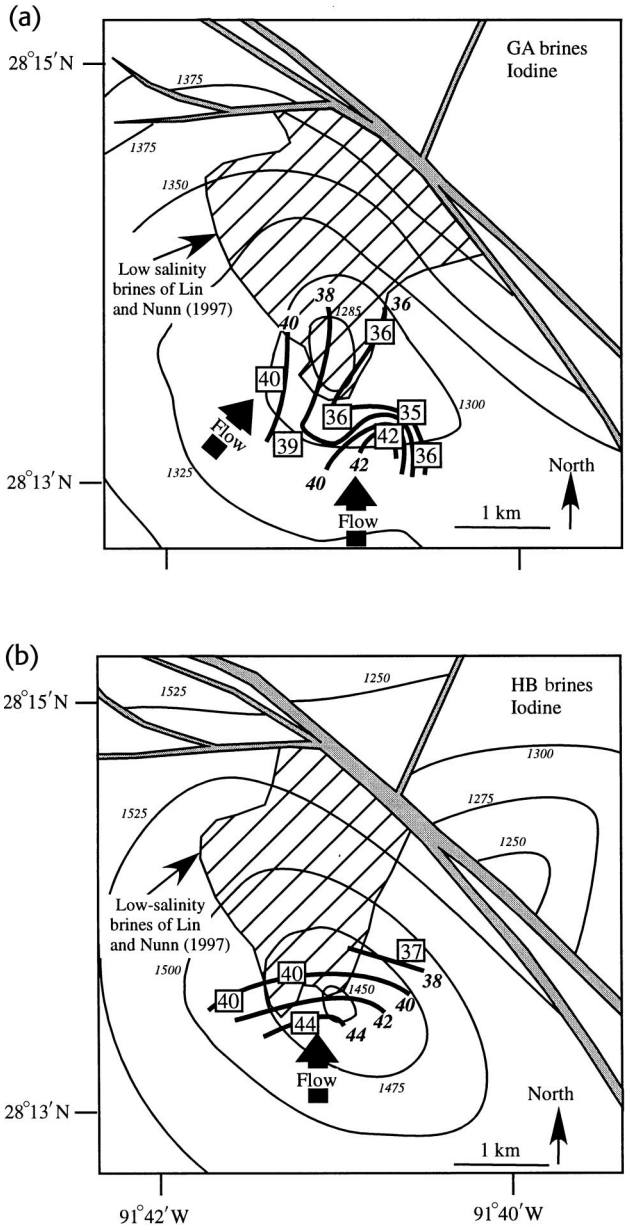

Figure 9. Structure contour map of top of (a) the GA sand and (b) the HB sand (both modified from Holland et al., 1990). Data points and contours (bold italics) for brine iodine concentration (mg/L) are shown. Iodine concentration decreases to the north in both reservoirs, suggesting dilution of deeply sourced, high-iodine brine with connate, low-iodine waters, consistent with brine flow from the south. So-called low salinity (<55,000 mg/L Cl^-) brines interpreted by Lin and Nunn (1997) from SP logs are shown for comparison.

fracture system, along which the composition of the brine was little modified from that at depth.

In summary, brine compositions in Block 330 are compatible with fluid sources in early Tertiary or older sediments, from which they ascended, variably

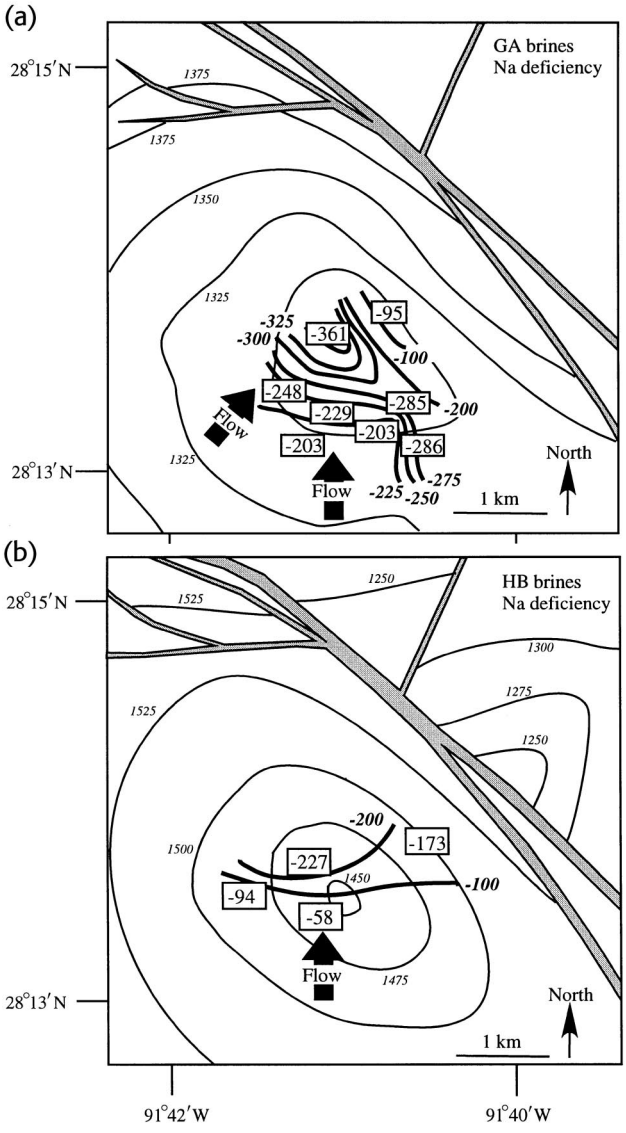

Figure 10. Structure contour map on top of (a) the GA sand and (b) the HB sand (both modified from Holland et al., 1990), showing data points and contours of sodium deficiency (mM). Values generally increase to the northeast (GA) to north (HB), indicating flow to the north.

dissolving salt (also see Land and MacPherson, 1989). Source of brines as indicated by $^{87}Sr/^{86}Sr$ compositions is corroborated by ^{129}I/total iodine ages for SEI330 brines, which range from 31 to 146 Ma, when corrected for probable input of ^{129}I from uranium decay in the sediments (Moran et al., 1995) (Table 1). Moran et al. (1995) interpreted the iodine isotopic data to indicate that the brines migrated vertically from the Eocene Wilcox Formation equivalent or older sediments.

The south to north increase of Na deficiency, which tracks brine-sediment interaction, suggests that the GA and HB brines flowed from the south. The brines were involved in significant cation exchange within the reservoirs, their $^{87}Sr/^{86}Sr$ ratios increasing with increased interaction with reservoir sediment. When they entered the reservoirs, the brines likely had low Mg^{2+} and K^{+}, owing to probable involvement in clay and carbonate mineral diagenesis at greater depth (Boles and Franks, 1979; Land et al., 1988; MacPherson, 1989). Upon entering the shallow, relatively cool reservoirs, the brines exchanged with clays that had not yet been significantly altered by diagenesis, particularly widespread transformation of smectite to illite (e.g., Milliken, 1985), and so exchanged Na^{+} for Mg^{2+} and K^{+} sufficient to produce concentrations similar to those of seawater. The significant differences in chloride content and ^{129}I ages within and between reservoirs (particularly the GA and HB sands) allow different brine sources to be identified and indicate that these brines followed different pathways to their respective reservoirs.

RESERVOIR OIL CHEMISTRY

Like the brines, some oil chemical parameters show differences between and within reservoirs. As is described in a following section, some of these parameters are source related, and some reflect processes that affected the oils to varying extents during migration. This section describes variations in V/Ni ratio and percent sulfur in the SEI330 oils, as well as the distribution of n-alkanes in, and their selective removal from, SEI330 oils by phase separation ("gas washing" of Meulbroek et al., 1998). The compositional data are then integrated into an understanding of the processes that affected oil composition and of the plumbing system by which fluid migrated into the reservoir sands.

Results of Oil Chemistry

General Oil Characteristics at SEI330

As reported by Whelan et al. (1994), Block 330 oils are of broadly similar maturity and source. All of the oils have maturity between 0.75 and 0.85% vitrinite reflectance (R_o) equivalent and sourced from marly carbonates of probable Jurassic (Smackover) age. Schumacher (1993) reported that oils are biodegraded and water washed in the upper two reservoirs (GA and HB), which are at temperatures of 50–55°C. This biodegradation is of moderate extent, as it affected only n-alkanes and isoprenoids but not C_{29} sterane isomers

(data in Whelan et al., 1994; Peters and Moldowan, 1993). Schumacher (1993) and Whelan et al. (1994) noted the presence of condensate or light oil in the GA and HB sands, overprinting the biodegraded oil background on gas chromatograms. Biodegradation, as indicated by a pristane/n-C_{17} ratio greater than 1.0 (Table 2) (Curiale and Bromley, 1996), diminishes markedly with depth (also see Whelan et al., 1994). On the downthrown side of the A fault, oils below 2040 m (~6700 ft), at temperatures of 65°C or hotter, are largely unbiodegraded regardless of reservoir (Figure 11).

Compositional Variations in Block 330 Oils

Although the Block 330 oils are broadly similar in terms of source and maturity, whole-oil data (Table 2) yield evidence of small but significant compositional differences between and within reservoirs, primarily in terms of V/Ni ratio, sulfur weight percent, and extent of fractionation of light n-alkanes by gas washing (Meulbroek et al., 1998). In addition, the oils show different initial (prefractionation) distributions of heavy vs. light n-alkanes, described in a following section.

V/Ni

The relative amount of the heavy metals vanadium and nickel in oil depends on the oxidation state during decomposition of organic matter in the source rock (Peters and Moldowan, 1993). The V/Ni ratio is not significantly affected by biodegradation or processes that alter oil composition during migration; thus, it reflects source. The V/Ni ratios of OI oils cluster in a narrow range (Table 2), whereas a wider range of V/Ni ratios exists in the GA and HB oils, indicating variability in source conditions. In the GA and HB sands, oil V/Ni generally increases from north to south (Figure 12).

n-Alkane Patterns of IC–OI Oils

Oil compositions can be described and compared by use of molar fraction plots (Kissin, 1987), in which the logarithm of the mole fraction of each n-alkane is plotted against the carbon number of that n-alkane (Figure 13). A normal oil that has not been affected by fractionation processes displays a straight-line fit on such a plot for carbon numbers greater than 9 or so, depending on separator and storage conditions (Kissin, 1987). For oils that have not undergone compositional modification after generation, the slope of this line is primarily a function of the maturity of the oil. Less mature oils have higher proportions of heavy n-alkanes to light ones; thus, they have a less negative slope on this plot. Block 330 oils divide into two basic compositional categories: relatively high sulfur oils that have n-alkane slopes of -0.15 to -0.19 and that are found mainly in the OI, NH, and IC sands and significantly lower sulfur oils that have n-alkane slopes of -0.20 to -0.25 and that are found mainly in the MG, LF, and KE sands (Table 3; Figure 14). Whelan et al (1994) showed that the lower sulfur content corresponds to higher API gravity in these oils. These differences may reflect small variations in the thermal maturity of the oils, slight differences in source rock characteristics, or variable involvement of oil with deep phase separation events.

In addition to the variability of n-alkane slopes shown by the different oils, the oils also exhibit variable amounts of selective depletion of relatively low molecular weight (gasoline range) n-alkanes. The preponderance of oils from reservoirs above the OI sand is characterized by a straight-line fit at carbon numbers greater than 7 (shown in Figure 13), hence showing no selective depletion of lighter n-alkanes. In contrast, nearly all of the OI oils showed pronounced deficiency of n-alkanes having carbon numbers from less than 10 to 16, depending on the sample. Compared with most of the shallower Block 330 oils, the OI oils are fractionated, probably as a result of gas washing (Meulbroek, 1997; Meulbroek et al., 1998).

Parameters related to the chemistry of the fractionated oils can be determined from the molar fraction plot, as shown in Figure 13. In particular, a quantity referred to by Meulbroek et al. (1998) as the "break number," or carbon number of the n-alkane where the best-fit curve to the data departs from a linear trend and which is a function of the physical conditions that prevailed during gas washing, can be determined visually. Maps of oil break numbers for each reservoir (Figure 15) illustrate that all OI oils are fractionated, whereas fractionated and unfractionated oils are mixed in overlying sands. Considerable lateral variability with respect to break number also exists within the OI sand. The GA and HB oils cannot be evaluated in this manner, owing to biodegradation of their n-alkanes.

Gas Source

Compound-specific isotopic data from gases collected in Block 330 (Table 4) were used by Whelan et al. (1994) to determine a range of maturities of 1.3–1.5% R_o for the gas source at the time of gas generation. The gas maturities show no distinction by reservoir. Further analysis of individual compound $\delta^{13}C$ values using the graphical method of Chung et al. (1988) was carried

Table 2. Oil Chemical Data Discussed in Text*

Sand	Well	Depth		$\delta^{13}C$**	S (wt. %)	Ni (ppm)	V (ppm)	V/Ni	Pr/n-C_{17}†
		Meters TVD	Feet						
GA-2	A13D	1310	4297	−26.65	0.88	3.76	5.6	1.49	–
GA-2	B16D	1289	4228	−27.45	1.11	4.88	10.22	2.09	0.90
GA-2	B18D	1297	4254	−27.1	1.23	5.32	11.62	2.18	–
GA-2	B1D	1280	4198	−27.05	1.19	4.88	10.36	2.12	0.41
GA-2	C10D	1284	4213	−27.1	1.08	4.47	10.58	2.37	–
GA-2	C13D	1288	4223	−27.0	1.0	3.39	8.95	2.64	–
GA-2	C15D	1283	4208	−26.65	1.04	4.12	9.42	2.29	–
GA-2	C1D	1280	4197	−26.95	0.94	4.49	8.73	1.94	–
GA-2	C2D	1308	4290	−26.9	0.87	4.01	7.07	1.76	–
GA-2	C5D	1298	4259	−26.8	0.87	4.11	5.95	1.45	2.50
GA-2	C6D	1282	4205	−26.7	0.91	4.27	7.05	1.65	–
HB-1	A13ST	1453	4765	−26.35	0.9	4.04	6.98	1.73	–
HB-1	A18D	1470	4821	−27.1	1.04	4.85	7.97	1.64	–
HB-1	A2	1453	4767	−27.35	0.98	4.62	10.66	2.31	–
HB-1	B17D	1470	4822	−26.85	1.29	5.77	10.59	1.84	–
HB-1	B18	1473	4833	−26.75	1.45	8.06	16.76	2.08	–
HB-1	B2ST	1453	4767	−27.15	1.29	6.52	12.33	1.89	–
HB-1	C2	1457	4779	−27.2	1.23	6.9	12.98	1.88	–
HB-1	C3D	1449	4754	−26.85	1.17	5.92	10.59	1.79	–
HB-1	C4E	1451	4759	−26.9	1.36	8.68	16.66	1.92	2.54
HB-1B/2	B16	1450	4757	−27.3	1.6	10	22.56	2.26	–
HB-3	B3ST	1493	4900	−27.25	1.26	7	14.51	2.07	–
IC	A10ST	~1753	5750	NA	NA	NA	NA	NA	0.79
IC	A8ST	~1707	5600	NA	NA	NA	NA	NA	1.10
IC	C11	1704	5588	NA	NA	NA	NA	NA	0.95
J-1-D	A19ST	1905	6250	−27.35	0.02	0	0	–	1.60
JD	B17	1853	6078	−26.95	0.01	0	0	–	0.48
JD	A5	1925	6315	NA	NA	NA	NA	NA	0.60
JD	B7	1910	6265	NA	NA	NA	NA	NA	0.60
JD	A11	1948	6391	NA	NA	NA	NA	NA	1.24
KE	C18	2034	6672	NA	NA	NA	NA	NA	1.71
LF	B4	2158	7078	−27.15	0.69	1.82	2.41	1.32	0.68
LF	B5ST	2073	6800	NA	NA	NA	NA	NA	0.92
LF	B6ST	~2103	~6900	NA	NA	NA	NA	NA	1.00
LF	B7	2084	6837	−26.85	0.03	–	0	–	0.58
MG-1-2	A20	2209	7247	−27.2	0.51	0.93	1.28	1.38	0.55
MG-1-2	B9D	2226	7302	−27.2	0.35	0.59	0.92	1.56	0.53
MG-4	B9	2263	7424	−26.3	0.32	–	0.71	–	0.53
MG	C15	1860	6100	NA	NA	NA	NA	NA	–
NH	B10ST	2032	6666	−27.3	1.09	5.28	10.1	1.91	0.50
NH	A3	2291	7514	NA	NA	NA	NA	NA	0.56
OI-1	B12D	2149	7050	−27.3	0.9	4.24	8.21	1.94	0.52
OI-1	B15D	2178	7145	−26.75	0.92	4.53	8.5	1.88	0.46
OI-1	C14D	2149	7048	−27	0.89	3.8	7.42	1.95	0.59
OI-1	C16	2213	7257	−27.25	0.95	3.61	7.9	2.19	0.40
OI-1	C17ST	2203	7226	−27.2	0.93	4.81	9.6	2	0.48

Table 2. Oil Chemical Data Discussed in Text (Continued)*

Sand	Well	Depth		$\delta^{13}C$**	S (wt. %)	Ni (ppm)	V (ppm)	V/Ni	Pr/n-C_{17}†
		Meters TVD	Feet						
OI-1	C4	1809	5933	NA	NA	NA	NA	NA	1.69
OI-1	C7A	2325	7616	−27.35	0.89	4.28	9.18	2.14	0.46
OI-1	C9D	2185	7168	−26.9	0.89	3.84	7.89	2.05	0.53
OI-1-2	A14A	2154	7066	−27	0.1	–	0.23	–	0.59
OI-1-2	A4	2384	7836	−26.75	0.03	0	0	–	0.56
OI2	A14	2180	7150	NA	NA	NA	NA	NA	0.56
OI2	B11	2146	7039	NA	NA	NA	NA	NA	0.60
OI2	B3	2264	7427	NA	NA	NA	NA	NA	0.51

*Analyses were performed at Texas A&M University (Whelan et al., 1994).
**Whole oil analysis; NA = not analyzed.
†Dash in Pr/n-C_{17} column indicates one or both peaks for pristane and n-C_{17} had a reported value of zero, owing to biodegradation.

out to determine the bacteriogenic methane fraction in each reservoir, to determine if the thermogenic gases in the different Block 330 reservoirs have a common source and to compare the calculated isotopic composition of the gas source with the $\delta^{13}C$ values of oil at Block 330. The compound $\delta^{13}C$ values were plotted vs. 1/carbon number of the analyzed n-alkane (Figure 16). For the several samples for which n-butane $\delta^{13}C$ was determined, a straight-line fit through the C_2–C_4 compounds implies isotopic equilibrium for those compounds. For most samples, only methane, ethane, and propane $\delta^{13}C$ values were available, but plots using these data yield the same trends as those plots that included n-butane data. On Figure 16, the extrapolation to methane gives the $\delta^{13}C$ value of pure thermogenic methane in isotopic equilibrium with the wet gas compounds. This value is used in estimating the fraction of bacteriogenic methane in the sample (Table 4). Extreme end-member bacteriogenic methane $\delta^{13}C$ values of −60 and −120‰ are used in the computation (Claypool and Kaplan, 1974); Land and MacPherson (1989) measured a value of −73‰ for bacteriogenic methane 8 km west of Block 330. On the plot, extrapolation to the ordinate gives the $\delta^{13}C$ value of an infinite carbon-number source for the gas (Chung et al., 1988), which approximates actual $\delta^{13}C$ of the gas source.

Application of the Chung et al. (1988) method to SEI330 gases indicates that the carbon isotopic composition of the gas source ranges from −22.8 to −25.8‰, with a mean of −23.8‰ (Table 4; Figure 17). This is several parts per thousand heavier than measured SEI330 whole-oil $\delta^{13}C$ values of −27.01 ± 0.2‰, indicating the gas and oil may have different sources. Bacteriogenic methane comprises 4–21% of the total methane fraction of the sampled gas (Table 4), given end-member bacteriogenic methane $\delta^{13}C$ of −120‰, or 14–69% of the total methane, given end-member bacteriogenic methane $\delta^{13}C$ of −60‰. We computed a similar range of bacteriogenic gas contents of Block 330 gases by means of the isotopic fractionation plot of James (1983).

OI-1 RESERVOIR PRESSURES

In addition to insights gained from oil and brine chemistry, the plumbing system that fed the Block 330

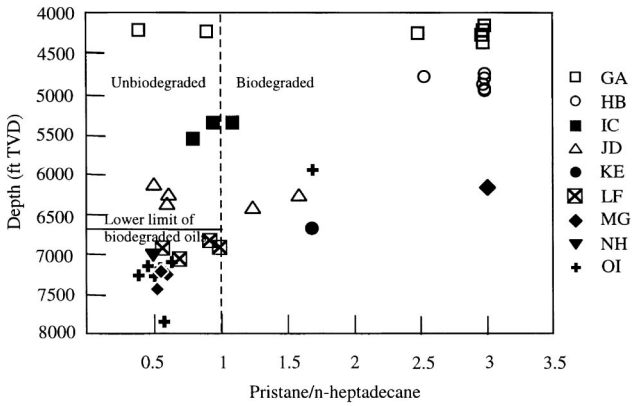

Figure 11. Pristane/n-heptadecane ratios for Block 330 oils. The lower limit of biodegraded oils (ratio > 1.0 [Curiale and Bromley, 1996]) is at 6700 ft (2042 m), corresponding to a temperature of 65°C. Indeterminate Pr/n-C_{17} ratios (Table 2) are plotted as a value of 3 on this plot for the sake of showing the distribution of biodegraded oils.

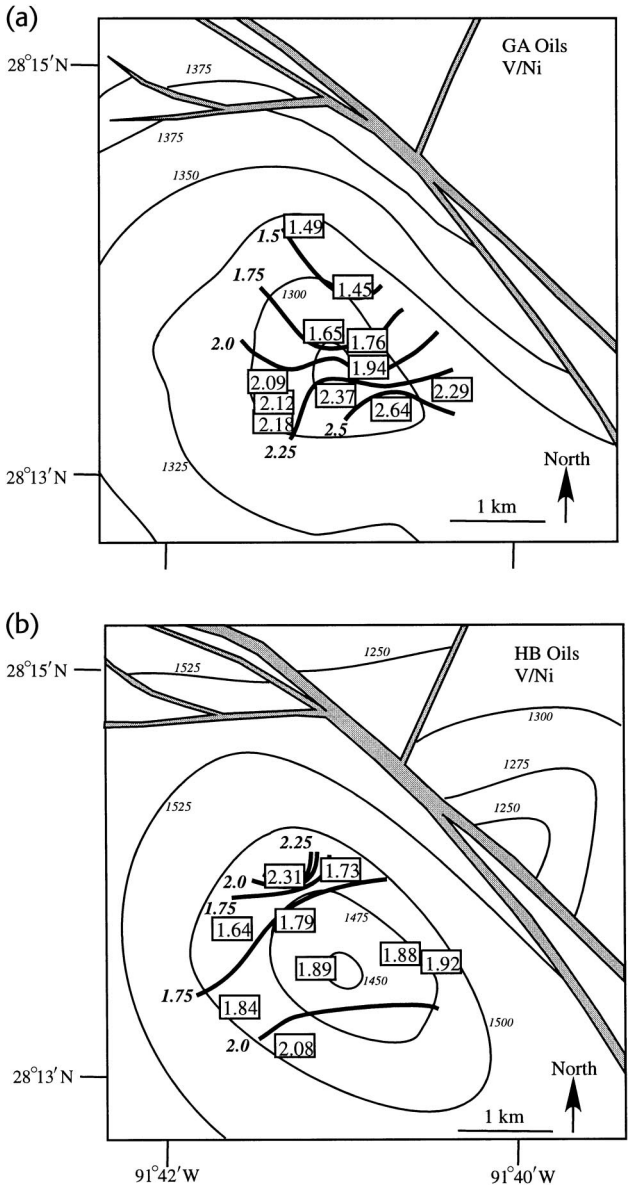

Figure 12. Structure contour map (in meters) of top of (a) the GA sand and (b) the HB sand showing V/Ni of oils. Both maps are modified from Holland et al. (1990). In both reservoirs, V/Ni and sulfur generally increase from north to south.

reservoirs can also be evaluated through the integration of hydrocarbon distribution and preproduction fluid pressure measurements between different fault blocks in a particular sand. In the OI-1 sand, the F fault separates oil (fault block A) from gas (fault block B). Displacement on this fault diminishes to nearly zero near the crest of the structure (Figure 18). At the depth of minimum offset, near the top of the hydrocarbon columns, the fluid pressure difference in the OI-1 sand across the F fault is small, about 130 ± 50 psi (Figure 19; data in Table 5), and increases downward. Thus, the two sands are nearly in hydraulic communication at the top of the structure. The near equality of pressure, given the large difference in column heights and compositions across the fault, is strongly suggestive of a leaky barrier. The 130 psi pressure differential probably represents the maximum sealing capacity of this fault, given the minimal displacement, and the fault probably leaks from fault block A into fault block B at higher pressure differential. The leakiness of this fault is a critical aspect of the filling model for the OI-1 sand presented in a following section of this article.

DISCUSSION

The data allow investigation of several issues of importance in determining the nature and geometry of fluid migration into the reservoirs, as well as evaluation of processes that affected the fluids during migration. We evaluate gas source, timing of hydrocarbon migration, reservoir continuity, and gas washing and present an integrated plumbing system model for the SEI330 reservoirs.

Gas Source

In general, there is no significant difference in calculated percentage of bacteriogenic gas between reservoirs (Table 4), nor is there a significant difference in carbon isotopic composition of thermogenic gas source between reservoirs. The same gas source fed all of the Block 330 sands. The gas may have sourced from cracking of Jurassic oils (Whelan, 1997), but the fact that these oils have $\delta^{13}C$ values of -27.0 (± 0.27)‰, slightly more than 3‰ lower than the gas source, suggests that the gases were more likely produced from Cretaceous or lowermost Tertiary sediments that are now in the gas window (Harrison and Summa, 1991; also see McBride et al., 1998). Alternatively, the gas was generated by cracking of oil still trapped in Mesozoic source rocks, after the SEI330 oils were generated and expelled. Such scenarios are compatible with the large difference in maturity between oil (0.8% equivalent vitrinite reflectance [R_e]) and gas (1.5% R_e) at SEI330. The oils must have migrated out of their source rock prior to generation of the SEI330 gas.

Incorporation of bacteriogenic gas into Gulf of Mexico gas reservoirs is common, as noted by Rice and Claypool (1981). Schoell and Beeunas (1996) noted that such gas is commonly found near faults in the Gulf of Mexico. At Block 330, low $\delta^{13}C$ methane is present

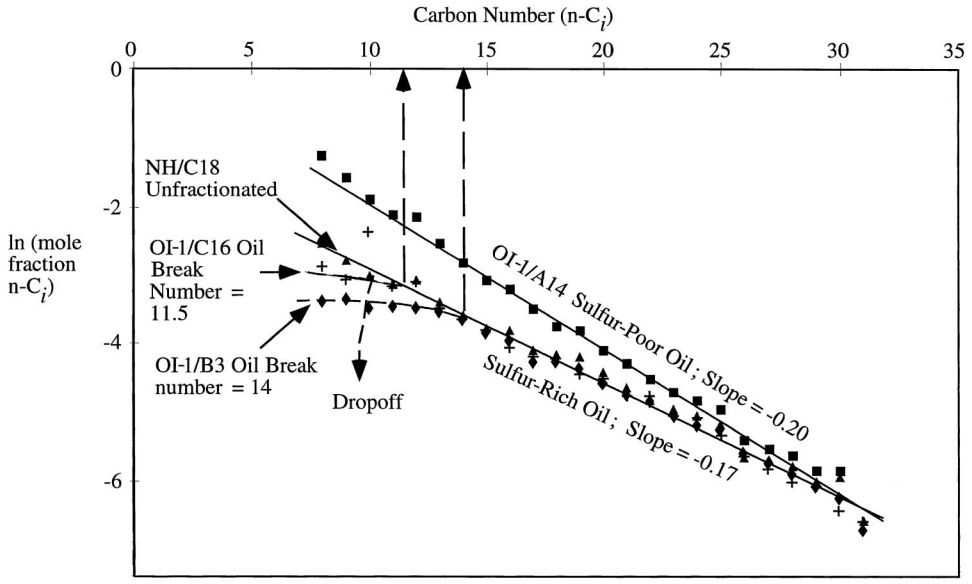

Figure 13. Molar fraction plot: natural logarithm of the mole fraction of each n-alkane vs. the carbon number of that n-alkane. Distinction is shown between unfractionated and fractionated oils. For fractionated oils, the break between depleted and undepleted parts of the n-alkane spectrum (break number) is shown. Curves have been shifted vertically to facilitate comparison of variably fractionated oils and between oils of different n-alkane slopes.

in the A6ST well, near the A fault (Table 4). Similar gas, of high bacteriogenic methane content, has been collected from the A fault zone 300 m from the A6ST fault cut (Losh et al., 1999), implying that bacteriogenic gas within the fault zone locally escaped into the reservoirs. This gas was presumably generated at shallow depth and was buried with the sediment. Such concentrations of bacteriogenic methane are uncommon at Block 330, however. In general, there is little variation in gas source or proportion of thermogenic vs. bacteriogenic methane throughout the reservoirs. Overall, the difference in gas source $\delta^{13}C$ and maturity relative to oil at Block 330 favors a model in which the two were generated separately and mixed late in the migration history, compatible with the gas-washing modeling results presented in a following section.

Timing of Reservoir Filling

Geological and geochemical data indicate that the Block 330 reservoirs filled relatively recently in the history of the minibasin (Holland et al., 1990; Anderson, 1993; Schumacher, 1993; Whelan et al., 1994; Alexander and Handschy, 1998; Losh, 1998). In addition to conventional methods of determining migration timing by evaluating when the traps formed, constraints on timing of reservoir filling can, in this instance, be obtained by examining the distribution of biodegraded oils in the stratigraphic section. The biodegraded GA and HB oils lie above unbiodegraded oils in the IC–OI sands, consistent with a temperature cutoff for bacterial activity in these oils (Whelan et al., 1994; Losh, 1998) (Figure 11). Other factors that affect the distribution of biodegraded oils, such as variations in brine chemistry, do not come into play in this field: the GA and HB brines clearly are not oxygenated or diluted fluids (i.e., mixed with meteoric water or downward-flowing seawater) that differ chemically from the deeper brines in the unbiodegraded reservoirs. In addition, the reservoir sand depositional environment does not differ significantly between reservoirs containing biodegraded as opposed to unbiodegraded oils. In particular, the GA, HB, and structurally high parts of the JD and OI reservoirs, which contain mildly biodegraded oil (Table 2), consist largely of deltaic sands (Alexander and Flemings, 1995; Hart et al., 1997). Thus, the distribution of biodegradation at Block 330 primarily reflects differences in temperature history, particularly the minimum temperature, experienced by the oils. The scarcity to absence of biodegraded oils in sands below about 2 km (6700 ft) suggests that sands deeper than this were filled primarily or exclusively at temperatures greater than 65°C. The maximum age of filling can then be approximated as the time the reservoir sand was buried through the 65°C isotherm. Using a sedimentation rate of 1.3 mm/yr for the late Pleistocene (based on Alexander and Flemings, 1995), the OI sand must have filled within the past 120 k.y., with the maximum filling age of the NH–IC sands being progressively younger. Accordingly, the JD sand filled within the past 50 k.y. If the JD condensate separated from the OI residual oils (Whelan et al., 1994) and both fluids then directly migrated to their respective sands, then filling of the OI sand, and by implication the entire

Table 3. n-Alkane Curve-Fitting Parameters for Block 330 Oil Samples

Well	Sand	Break No.*	Slope**
C9D	OI-1	13.8	−0.15
C21	OI-1	13.5	−0.16
B11	OI-2-FB-A	15.9	−0.19
B11D	OI-1	13	−0.19
B13D	OI-1-FB-A	13.1	−0.18
B3	OI-1	14	−0.17
A2ST	OI-5-FB-D	13.6	−0.20
A14	OI-2	U	−0.20
C19	OI-1	13.1	−0.18
B12D	OI-1	12.6	−0.17
B15D	OI-1	13.0	−0.18
C7A	OI-1	13	−0.17
C14D	OI-1	13.0	−0.18
C16	OI-1	11.6	−0.17
C17ST	OI-1	13	−0.17
A4	OI-1-2	9.6	−0.73 (Cond)
B10ST	NH-FB-A1	U	−0.15
A3	NH	U	−0.20
C18	NH	U	−0.16
B10ST	NH	U	−0.16
C15	MG	U	−0.75 (Cond)
A20	MG-1-2	10.5	−0.22
B9D	MG-1-2	U	−0.21
B9	MG-4	U	−0.23
B5ST	LF	U	−0.25
B6ST	LF-FB-A	U	−0.22
A21	LF-FB-B	15.0	−0.18
B-14D	LF	13.9	−0.20
B4	LF	U	−0.20
B7	LF	U	−0.64 (Cond)
A5	KE-2	U	−0.89 (Cond)
A6ST	KE-FB-E	U	−0.95 (Cond)
C17A	KE-2	U	−0.73 (Cond)
C18	KE-2	U	−0.22
B7AST	JD-FB-A	U	−0.23
A1B	JD-FB-B	U	−0.89 (Cond)
A5D	JD	U	−0.94 (Cond)
A11D	JD	U	−0.48 (Cond)
A19ST	J-1-D	U	−1.02 (Cond)
B7A	JD	U	−0.94 (Cond)
B17	JD	U	−1.02 (Cond)
A8ST	IC-4	U	−0.19
A10ST	IC-4	U	−0.18
C11	IC-4	U	−0.21

*U = a break number less than 9.0. For all practical purposes, an oil with a break number higher than 9 has been affected by gas washing, as opposed to migration fractionation, alteration due to phase separation during production, geochromatography, and diffusion (Meulbroek et al., 1998).

**Cond = gas condensate, the liquid that condensed from a vapor phase at the separator.

reservoir sequence, also occurred within the past 50 k.y. Thus, most of the oil and gas migration into the Block 330 reservoirs certainly occurred within the past 1 m.y. (the GA sand is 900 ka), very likely within the past 120 k.y., and possibly within the past 50 k.y. The reservoir filling is thus much younger than formation of the salt weld at 1 Ma or earlier. The large timing discrepancy is not likely caused by a long migration distance from the salt weld to the reservoirs, as the weld is only 1.5 km below the OI sand at the eastern end of the minibasin (Alexander and Flemings, 1995).

As noted by Schumacher (1993) and Whelan et al. (1994), unbiodegraded light oil or condensate is mixed with biodegraded GA and HB oils. Migration of these lighter fluids into the GA and HB sands postdates migration of the oil, as the condensates overprint a biodegraded background. This late charge may have migrated via the fault system from below the reservoir section (Whelan et al., 1994), or it may represent rapid leakage of gas condensate from the underlying JD sand.

Reservoir Geology: Continuity of Migration Pathways in the Sands

Hart et al. (1997) described the GA sand as a complex reservoir in which along-strata permeability is impeded by debris flows at the base of the sand. In addition, along-strata fluid flow is hindered by clayey drapes on foreset beds, which may act as baffles, particularly in southern Block 330 and in Block 338. These baffles have produced compartmentation of GA reservoirs in Block 338. Sand continuity improves near the crest of the Block 330 anticline, where mouth-bar sands are predominant. Hart et al. (1997) also documented that the net GA sand thickness decreases from 90 ft (27 m) at the crest of the structure to about 60 ft (18 m) at the antithetic fault in Block 338. In contrast to the stratigraphic complexity of this sand, the regular geochemical patterns across the reservoir imply filling by means of a uniform charge migrating from the south without evidence of compartmentation. Filling at geologic rates, over a time interval of tens to hundreds of thousands of years, may be largely unaffected by these stratigraphic barriers, which do exert strong lateral permeability control at production timescales, perhaps owing to large production-induced pressure transients. The hypothesis of filling from the south could be confirmed by documenting the existence of minor hydrocarbon accumulations or oil-stained sediments low on the structure, south of the GA and HB reservoirs in Block 330. Minor amounts of oil may be trapped at stratigraphic barriers identified by Hart et al. (1997)

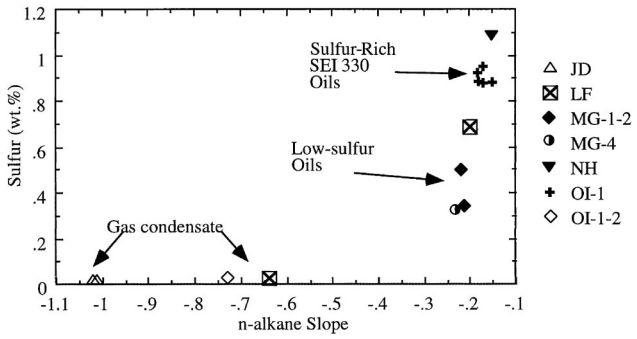

Figure 14. Whole-oil weight percent sulfur vs. n-alkane slope from molar fraction plot. Sulfur content strongly correlates with n-alkane distribution, compatible with a single source for the oils (as also determined from biomarkers) and a single process, probably thermal maturation, controlling both sulfur content and n-alkane slope.

and may be discernible as seismic amplitude anomalies. These barriers, however, did not significantly impede migration of the oils found in the GA and HB sands in Block 330.

For other sands in Block 330, net sand thickness maps (Holland et al., 1990) indicate existence of sand southward to the antithetic fault throughout the entire reservoir section. The LF and MG sands thin onto the anticline (Holland et al., 1990) but nonetheless are continuous to the south. Given that filling from the south is viable in the stratigraphically complex GA sand, similar migration pathways are very likely to exist for the other reservoirs as well.

Modeling of Gas Washing at Block 330

Price et al. (1983) demonstrated that crude oil may have significant solubility in methane gas. In Thompson's (1987) evaporative fractionation scheme, gas mixes with and dissolves some fraction of a liquid oil, producing a gas condensate and a residual oil. Experiments by Larter and Mills (1991) showed that mixing of partially miscible hydrocarbon fluids can result in fluids that resemble gas condensates found in nature. Building on these studies, Meulbroek (1997) and Meulbroek et al. (1998) demonstrated that the fractionated Block 330 oils had been subjected to gas washing: the continual interaction of gas with liquid oil, removal of components from the oil on the basis of their fugacity in the vapor phase, and subsequent separation of the vapor from the washed liquid. The vapor may later condense liquids as it flows to lower pressure and lower temperature. The compositional effects of gas washing on oil as a function of pressure, temperature, and initial system composition have been numerically simulated by Meulbroek (1997) and Meulbroek et al. (1998).

In previous articles, Meulbroek (1997) and Meulbroek et al. (1998) computed the pressure-temperature-compositional (P-T-x) conditions of gas washing at Block 330 on the basis of plots of break number vs. oil paraffinicity or aromaticity as defined by Thompson (1987). However, these latter parameters are subject to modification by processes other than gas washing and, furthermore, show variability related to initial compositional differences between oils. To improve the accuracy of the P-T-x computations, parameters related only to gas washing were used in the present computations. Recalibration of the model to accommodate the change in input parameters resulted in our interpreting the depth of gas washing of the fractionated oils at Block 330 to be between 2.4 and 2.9 km, based on the current fluid pressure profile and geothermal gradient. If gas washing occurred within the past 120 k.y. (see previous sections), the present depth of the sediments in which washing occurred would be 2.6–3.1 km, based on sedimentation rates from Alexander and Flemings (1995). These fractionation depths are greater than the deepest OI reservoirs, which presently lie at 2.1–2.4 km, and instead are centered on the Lentic sand, a slope fan approximately 600 m below the OI sand (Figure 2). The OI oils interacted with a mobile vapor phase along their migration pathway at the depth of the Lentic sand and separated from it prior to entering the OI sand. Calculated molar gas:oil ratios are between 9:1 and 14:1, averaging 12:1, in agreement with ratios reported by Meulbroek et al. (1998). In terms of volumes at reservoir conditions, this latter ratio translates to about 18 volumes of gas per volume of oil.

Other possible explanations for the observed light end depletion of the OI oils do not appear viable. (1) Modeling results show that separation of a saturated vapor phase at current reservoir conditions (e.g., gas cap separation, migration fractionation) (Silverman, 1965) would result in the removal of n-alkanes up to only n-C_9 and thus would not account for the observed removal of compounds as heavy as n-C_{15}. This requires significantly higher pressures than those that currently prevail in the reservoirs. Furthermore, gas cap separation does not remove nearly enough light gasoline–range n-alkanes to produce the mass deficiencies that are observed in the OI oils. (2) Biodegradation, which is known to affect n-alkanes in the same range as gas washing, is ruled out for these oils on the basis of their

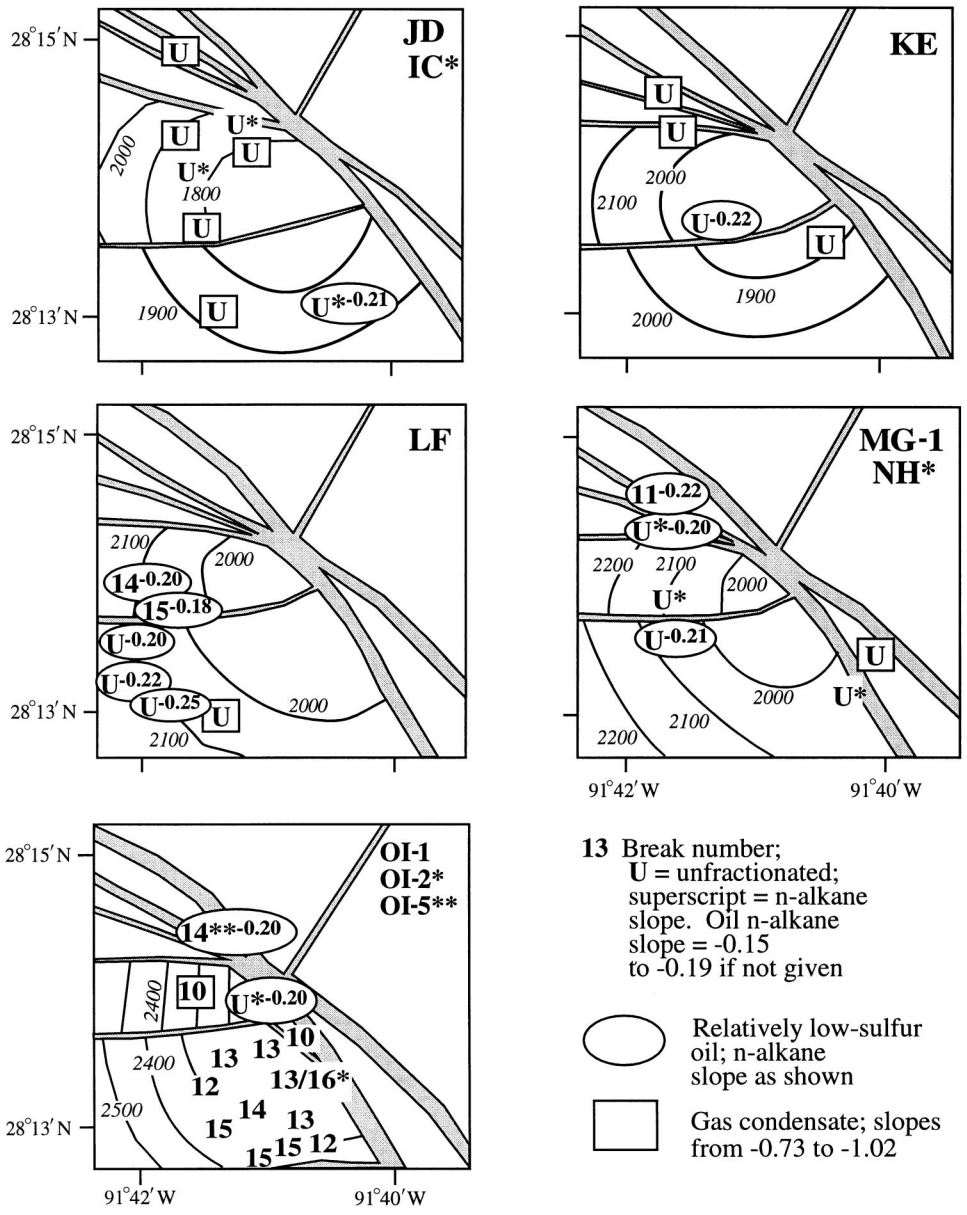

Figure 15. Structure contour maps (depths in meters) of Block 330 sands, showing break numbers and n-alkane slopes of oils from the indicated reservoirs. Outline of SEI330 is shown. The OI oils are distinct from all others, in that they have low slopes (-0.16 to -0.19) and are fractionated. Oils having n-alkane slopes similar to OI oils are present in the NH and IC reservoirs; however, these oils are not fractionated.

low pristane/n-C_{17} ratios (see also Whelan et al., 1994). In addition, gas washing removes compounds in order of their fugacity in the vapor phase, a pattern not readily produced by biodegradation. (3) The OI-1 sand in fault block A had been subjected to injection of 29 bscf (billion standard cubic feet) gas into the crest of the structure in the 1980s (Holland et al., 1990), to increase reservoir pressure and, in the process, produce a gas cap. However, no gas cap was produced, and no increase in gas production was noted in downdip OI-1 wells in fault block A (D. Pettus, 1999, personal communication); thus, the injected gas did not wash the bulk of OI-1 oil in fault block A. In addition, significant gas washing is documented for oils from other Block 330 reservoirs, where no gas injection program was implemented. (4) In-situ gas washing would result in a pattern whereby break number, which tracks pressure of phase separation, would increase with depth. Figure 15 shows this clearly is not the case for the OI oils. Gas is not currently washing the OI oils to any significant extent, and, furthermore, significant present-day gas washing at SEI330 in general is precluded by the abundance of unfractionated oils in the shallower reservoirs.

Plumbing Systems for OI–JD Sands

The migration pathways to and within the OI, MG, LF, KE, and JD sands are largely identified on the basis

Table 4. Compound-Specific Gas Isotope Data for Block 330*

		$\delta^{13}C$ (‰)**					Bacteriogenic C_1 (%)†	
Sand	Well	C_1	C_2	C_3	n-C_4	Gas Source	−60††	−120‡
GA	C13	−42.0	−28.8	−26.9	–	−23.0	31	9
HB	B18	−40.7	−28.7	−27.6	–	−25.8	31	10
	C5	–	−27.8	−26.2	−25.5	−23.2	–	–
JD	B17	−37.2	−28.3	−26.8	–	−24.0	17	5
	A1B	−36.3	−28.7	−27.3	–	−24.2	12	4
	A11B	−39.4	−28.4	−26.7	–	−23.1	22	7
	C8D	−39.5	−28.7	−26.6	−26.2	−24.4	30	10
	C8D2	−39.1	−27.6	−27.1	–	−23.8	21	6
	B7A	−38.1	−28.3	−26.8	–	−23.8	20	6
JD/KE	A6ST	−51.7	−29.8	−27.3	−26.7	−23.6	69	21
KE	A5	−40.4	−27.4	−26.4	–	−24.3	34	11
MG	C8	−36.8	−28.3	−26.8	–	−24.0	15	5
OI	B12(1)	−38.7	−28.0	−26.7	–	−23.7	23	7
	B12(2)	−36.5	−28.3	−26.6	–	−23.9	14	4
	C7	−37.8	−28.1	−26.7	–	−23.8	20	6
	C14	–	−24.3	−23.7	−24.1	−22.8	–	–

*Samples were analyzed at Texas A&M University (Whelan et al., 1994).
**$\delta^{13}C$ values relative to PDB standard.
†Method of Chung et al., 1988.
††Highest $\delta^{13}C$ value used for bacteriogenic gas end member.
‡Lowest $\delta^{13}C$ value used for bacteriogenic gas end member.

of oil and gas chemistry and on hydrocarbon distribution within the respective sands. As described in a previous section there are two main types of oil: a relatively low-sulfur type ($S < 0.6$ wt. %), having n-alkane slopes equal to or more negative than −0.20, and a relatively high-sulfur type ($S > 1.0\%$), having n-alkane slopes less negative than −0.20. Some of each of these oils has been gas washed below the present reservoir depths.

Filling of the OI and JD Sands: Gas-Washed, "Sulfur-Rich" Oil Plumbing System

As described in a previous section, the OI-1 sand contains relatively high-sulfur, gas-washed oil in fault block A and a large gas column (550 m [1800 ft]) with evaporative condensates in fault block B, with a much smaller oil leg than in fault block A (see Figure 1). These two columns have similar pressures at their tops (Figure 19) and are separated by a leaky fault. The distribution of hydrocarbons and the initial pressures in fault block A relative to fault block B indicates these fault blocks filled from the south (Figure 20). Gas that washed oil initially filled the OI-1 sand in fault block A and fault block B. Subsequent injection of the washed oil into fault block A from the south displaced the gas cap in fault block A across the leaky fault into fault block B, depressing the hydrocarbon-water contact there and spilling across a minor fault into fault block C (FBC in Figure 1). The evaporative condensate in the OI-1 sand in fault block B is probably a product of the gas-washing system that produced the JD condensate. Most of the vapor migrated to the JD and, to a lesser extent, the KE sands, presumably along the same fault zone as that which fed the OI sand from the south. Gas-washed, relatively sulfur-rich OI-1 oils

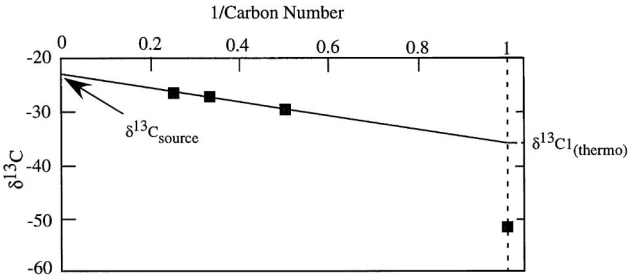

Figure 16. Rationale for interpreting gas isotope data, according to the method of Chung et al. (1988), as discussed in text. Sample A6ST (JD/KE sand) is shown.

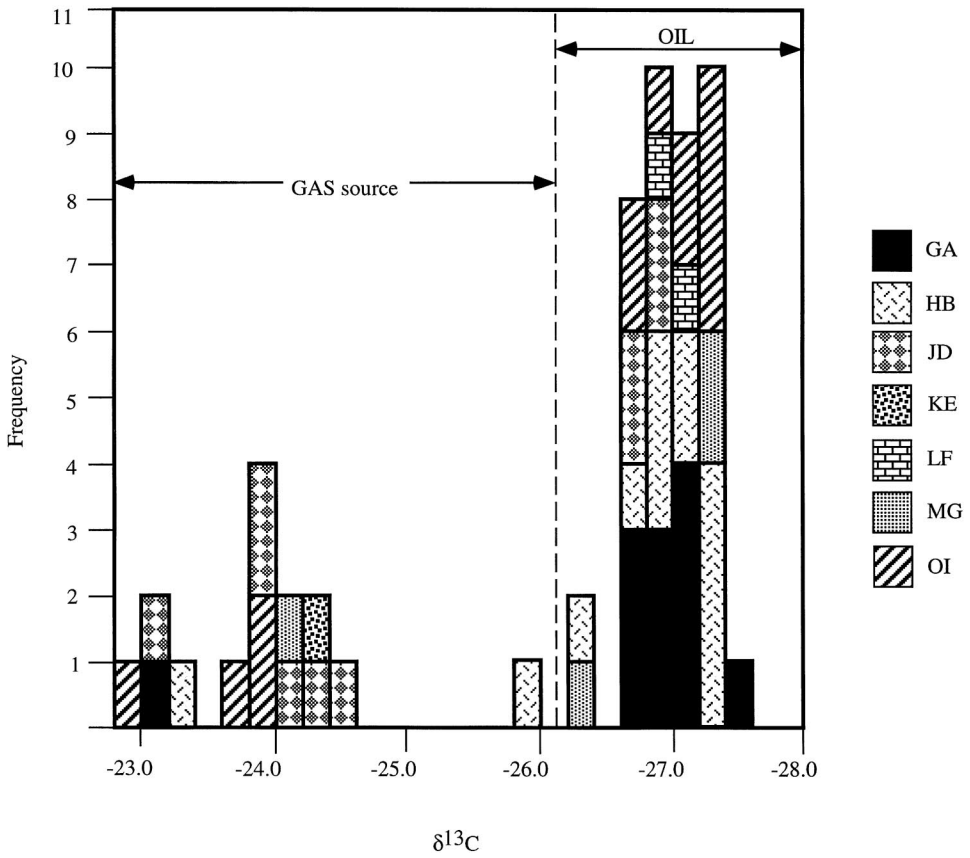

Figure 17. Histogram of gas source $\delta^{13}C$ values calculated according to the method of Chung et al. (1988). Patterns correspond to specific reservoir sands (GA–OI), as shown on right. For gases, the standard deviation of the 15 determinations is 0.7‰, and the mean is −23.8‰. Block 330 oil $\delta^{13}C$ values are shown for comparison and are on average 3‰ lighter than the calculated gas source $\delta^{13}C$ values. This difference implies that the oils and gases at Block 330 have different sources.

are not present in overlying reservoirs, indicating the uniqueness of the plumbing system that fed the OI-1 sand and also providing evidence that, contrary to the suggestion of Finkbeiner et al. (2001), OI-1 oils have not migrated to shallower reservoirs since filling.

Gas-Washed, "Sulfur-Poor" Oil

Gas-washed, sulfur-poor oil (n-alkane slopes of −0.20 to −0.25) is found in the LF, MG, OI-2, and OI-5 sands (Figure 15). With the exception of the OI-2 sample, all of the gas-washed, sulfur-poor oils are in the northern part of fault block B. These oils probably migrated into their respective sands from the north, as they are not known in fault block A to the south.

Filling of the MG, LF, and KE Sands: Unfractionated, "Sulfur-Poor" Oil Plumbing System

Alexander and Handschy (1998) identified the F fault as sealing in the MG and LF sands, on the basis of interpreted differences in oil chemistry across the fault. Our geochemical study corroborates their findings. In particular, LF oils in fault block A have higher n-alkane slopes, corresponding to lower sulfur, than LF oils in fault block B. Sufficient data do not exist to evaluate chemical variations in MG oils. The fractionated LF oils in the northern part of fault block B probably migrated from the north; thus, all LF oils in this fault block may have come from this direction. In contrast, the compositionally different LF oils in fault block A probably migrated from the south. The F fault, which leaks in the gas leg, allowed pressure equilibration of hydrocarbon columns in the LF sand. A similar filling model may apply to the MG and KE sands. In contrast to the OI oils, however, the MG, LF, and KE oils have relatively low sulfur content and steeper n-alkane slopes and thus represent influx from different accumulations, which fed the reservoirs along different migration paths than those taken by the OI oils.

The IC Sand: A Reservoir Containing Unfractionated, "Sulfur-Rich" Oil

Two oil samples in the discontinuous IC reservoir have an initial distribution of n-alkanes identical with the OI oils (slope of −0.16 to −0.19), but they are not gas washed (Table 3; Figure 15). Similar oil is found in the NH reservoir. The filling direction or history of these oils is not known, but it is different from that of any other Block 330 oil. The strong lateral fluid-pressure

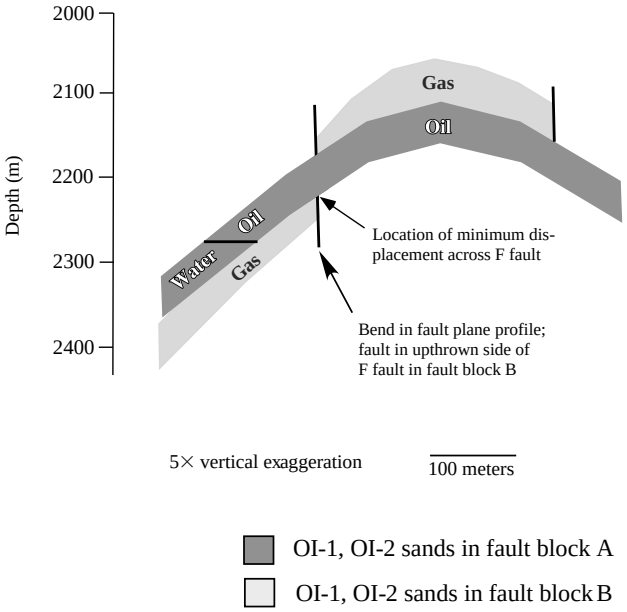

Figure 18. Fault plane profile for OI-1 and OI-2 sands, F fault and unnamed fault at crest of anticline (Figure 1), looking north. Dark shading corresponds to fault block A; lighter shading corresponds to fault block B. Fluid types and contacts are identified directly on the fault plane profile. Figure is based on structure contour maps of Pennzoil (now Devon Energy, 1992, unpublished data). Fault plane profile bends at fault intersection in fault block B.

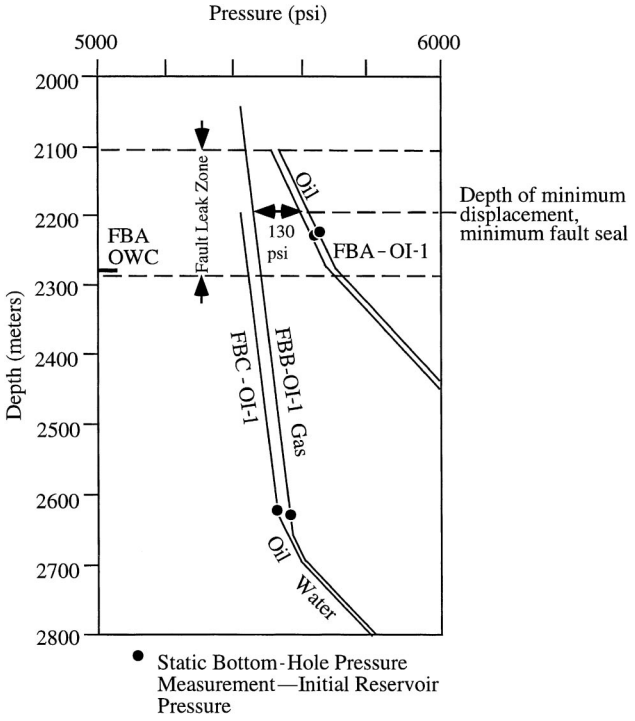

Figure 19. Fluid pressure vs. depth, OI-1 and OI-2 sands, Blocks 330 and 331. Pressures are projected to top of columns in respective fault blocks as shown using static bottom-hole pressure measurements combined with a water density gradient of 0.46 psi/ft, a live oil gradient of 0.30 psi/ft, and a gas gradient of 0.09 psi/ft. Fault block A (oil column) is separated from fault block B (large gas column) by the leaky F fault, which supports a fluid pressure difference of about 130 psi across the lowest displacement part of the fault.

gradient at the A fault, and the presence of oil in the fault zone in the A10ST well just below the IC-4 sand (Anderson et al., 1994a), suggest that the IC oils may have migrated via the A fault and filled from the northeast. A third IC oil, in the southern part of Block 330, is relatively deficient in sulfur and may reflect input from the south from the same system that fed this type of oil into the MG and LF sands.

SUMMARY AND CONCLUSIONS

Fluids migrated to the reservoirs at SEI330 from several locations and by a variety of pathways. They were modified by a variety of processes both prior to and synchronous with their entering the reservoirs. These components of the petroleum system are depicted in Figure 21 in terms of reservoir geometry and composition (Figure 21a), brine sources and pathways (Figure 21b), and hydrocarbon sources, pathways, and migration-related processes (Figure 21c). Block 330 reservoir brines originated from early Tertiary–Mesozoic sediments; their low Ca and Br contents preclude their sourcing as evaporative brines. The brines are all high in iodine, pointing to origin in sediments that have undergone catagenesis, hence below the present reservoir section. The ^{129}I dating permits the identification of two distinct sources in terms of age, shown on Figure 21b as "younger" and "older" brines (also see Figure 8).

Table 5. Preproduction Fluid Pressures for OI-1 and OI-2 sands, Blocks 330 and 331

Block/Well	Fault Block	Depth		Pressure (psig)
		Meters	Feet	
331/A7	B	2630	8625	5571
331/A18	C	2624	8608	5519
330/B3	A	2226	7300 (Datum)*	5652
330/C9	A	2226	7300 (Datum)**	5642

*Depth of measurement 2257 m (7403 ft). Pressure available only at datum.
**Depth of measurement 2214 m (7261 ft). Pressure available only at datum.

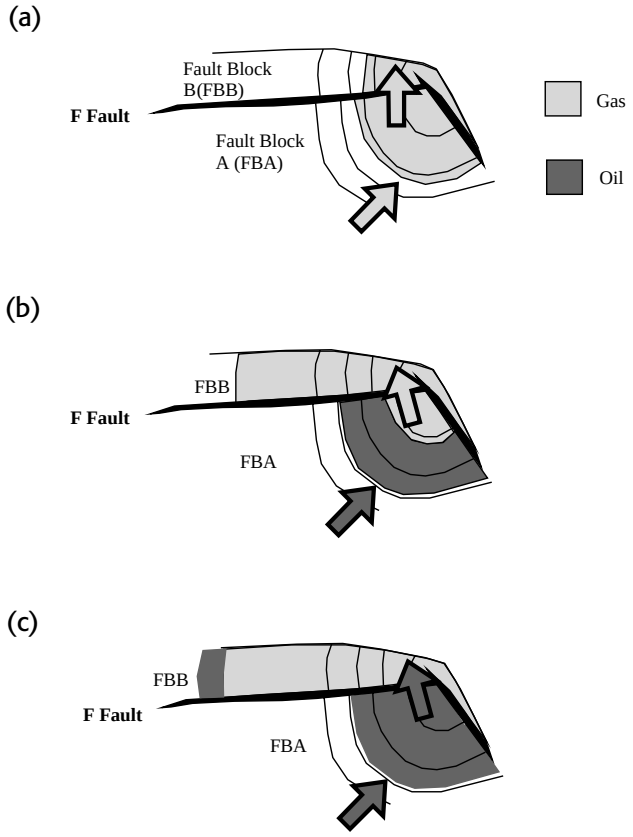

Figure 20. Interpreted filling history for the OI-1 sand. (a) Gas (from gas-washing event) fills first. Gas-water contacts are schematic. (b) Gas-washed oil follows, displacing gas across leaky F fault. (c) Fault block A is filled with oil. North is at the top of the map (see Figure 1).

Some of each brine type flowed past and dissolved salt prior to entering the reservoirs. In addition, the brines likely equilibrated with siliciclastic sediments during diagenesis at relatively high (>100°C) temperatures, causing depletion in Mg and K. The low $^{87}Sr/^{86}Sr$ endpoint ratio indicates that the brines did not interact much with sediment en route from their sources to the Block 330 reservoirs. The fluids probably ascended along faults bounding the minibasin. Once in the reservoirs, the brines exchanged Na for Ca, Mg, K, Ba, and Sr, primarily from clays. Dissolution reactions in the reservoir probably were a secondary factor in modifying brine composition. Progressive exchange of sodium as brine flowed across the GA and HB reservoirs, correlated with iodine-mixing trends in the reservoirs and with zonation of oil chemistry, indicates the brines in those sands likely flowed from the south. Different brines filled different sands, demonstrating the complexity of the plumbing system.

Oil was probably generated from various facies within Jurassic–Early Cretaceous marls presently 12–14 km below the surface and has ascended in such a way as to keep pace with basin subsidence. Gas was generated from a different source, probably by cracking of oil in situ, and mixed with the migrating oil, enhancing its ascent by reducing the viscosity and density of the liquid. Oils ascended to the reservoirs via both the A fault and the antithetic fault. Fluid pressure and hydrocarbon distribution indicate that the OI reservoir, for instance, filled mainly from the antithetic fault to the south. Slightly below the OI sand, some of these oils, including all those that are now in the OI sand, were gas washed as they were migrating. The vapor phase that resulted from this washing migrated primarily into the JD and, to a lesser extent, the KE sands. Equation of state modeling of this gas-washing event indicates that the cumulative volumetric gas:oil ratio during phase separation, at reservoir conditions, was about 18:1. Distribution of biodegraded vs. unbiodegraded oils at Block 330 indicates that the main reservoir section filled within the past 120 k.y., much more recently than the main phase of minibasin subsidence and salt weld formation.

As described, brine and oil chemical compositions indicate differences between GA, HB, JD, KE-NH, and OI reservoir fluids. These differences are not explicable by any single migration process but instead reflect slight differences in source and/or migration pathway to the reservoirs. It is generally agreed that the bulk of oil and gas migration into the Block 330 reservoirs was by means of the growth-fault system that bounds the reservoirs (Holland et al., 1990; Anderson et al., 1994a, b; Alexander and Handschy, 1998; Losh 1998; Losh et al., 1999). Brine geochemical zonation and hydrocarbon distribution indicate that cross-fault filling from the northeastern, upthrown side of the A fault in Block 330 is at best minor in comparison to flow up the faults. Below the minibasin salt weld, fluid migration pathways necessarily depart from the listric fault system that bounds the minibasin: oils migrated vertically from depths of 12–14 km, and brines sourced in Oligocene–Paleocene sands at least 8 km deep. Thus, the fluid sources and pathways discussed in this article can be envisioned as converging upward on the A fault–antithetic fault system, entering and ascending along it at different places and exiting at reservoirs when and where mechanical and geometric conditions were favorable (Losh et al., 1999). The fault zones, which are on the order of 100 m wide at the depth of the reservoir section, act to connect specific fluid

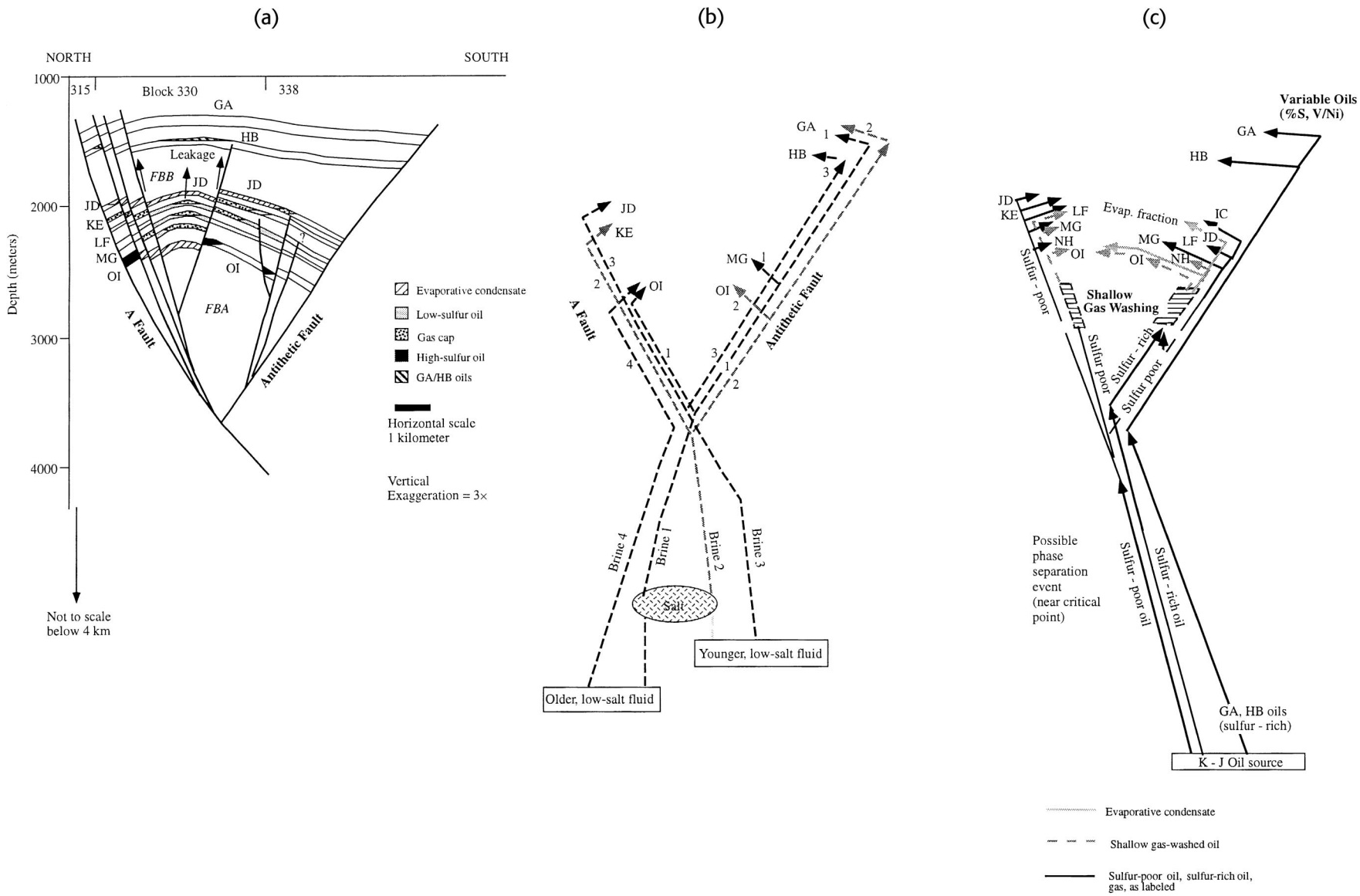

Figure 21. North-south cross sections through SEI330 reservoirs, as described in text, showing (a) geology, with fluid types currently in reservoirs, (b) interpreted brine pathways, and (c) interpreted hydrocarbon pathways and migration processes. Scale is the same for all figures.

accumulations at depth with specific reservoirs farther upstructure (Figure 22).

This analysis of migration pathways and processes that affect the chemistry of oil during its migration at SEI330 provides several tools that can be used in exploration in a variety of settings. The use of chemical indices that indicate flow direction in reservoirs can lead to discovery of other hydrocarbon accumulations upstream of known production. In addition, the analysis of gas washing, in which oil chemistry is combined with fluid-pressure evolution, burial history, migration timing, and equation of state and phase equilibria modeling of the gas-oil system, can identify deep sands (in this case, the Lentic sand) in which gas washing has occurred (see also Losh et al., 2002). If traps can be identified, these sands have a high probability of containing hydrocarbons.

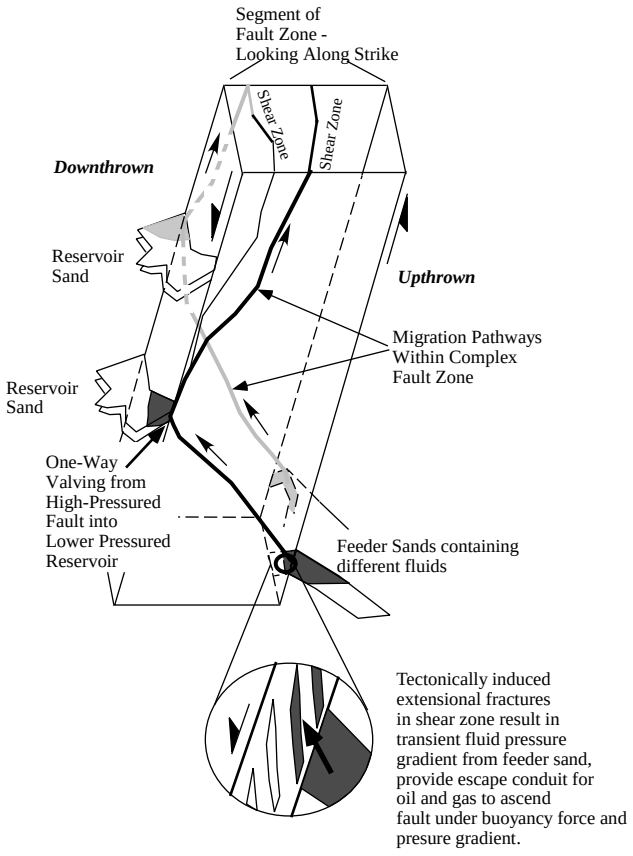

Figure 22. Schematic block diagram of fault zone, illustrating conduits in the fault zone connecting deep accumulations with shallower reservoirs. Fault transmits fluid when slip events occur.

APPENDIX: BRINE SAMPLING AND ANALYTICAL PROCEDURES

Temperature and pH measurements were made immediately on the platform. Water samples for carbon isotopic and dissolved inorganic carbon analysis were filtered, bottled, preserved with Zephiran chloride to prevent biodegradation, and refrigerated immediately. Samples intended for cation measurements were acidified to pH <2 with HNO_3 and analyzed by inductively coupled plasma atomic emissions spectrometry (ICP-AES) using a Leeman Labs PlasmaSpec III instrument. Anions were measured on a Dionex 4000i series ion chromatograph (IC) using AS2, AS5, and AS10 columns with suppressed conductivity for ultraviolet detection. Alkalinity was measured in the laboratory by electrometric endpoint titration using an automated titration system. Within-batch precision for elemental analyses (ICP-AES and IC), measured by gravimetric standards, ranged from $\pm 2\%$ for major elements to $\pm 5\%$ for trace elements. Samples were prepared for isotopic analysis according to techniques of Socki et al. (1992) and Venneman and O'Neil (1993).

Carbon Isotope Composition

The carbon isotope composition of dissolved inorganic carbon was determined on a subset of six samples that were preserved with Zephiran chloride and stored in serum vials capped with a Teflon septum. Off-line CO_2 extraction used a nitrogen-purged syringe and subsequent addition of phosphoric acid in vacuo. The carbon isotopic analyses were made on a Finnigan Mat-Delta S mass spectrometer with an analytical uncertainly of $\pm 0.10‰$. Carbon isotope compositions are given in the standard δ notation relative to Peedee belemnite (PDB).

Strontium Isotopic Measurements

Strontium isotopic compositions were determined on a subset of six brines. Standard ion-exchange procedures, using approximately 0.1 ml Sr-spec cation exchange resin, separated Sr^{2+} from water samples for isotopic analysis. All measurements were made on a VG Sector thermal ionization multicollector mass spectrometer. During the course of this study, the average $^{87}Sr/^{86}Sr$ value of NIST SRM-987 was 0.710245 ($2\sigma = 0.000040$).

REFERENCES CITED

Alexander, L., and P. Flemings, 1995, Geologic evolution of a Pliocene–Pleistocene salt withdrawal mini-basin, Eugene Island, Block 330, offshore Louisiana: AAPG Bulletin, v. 79, p. 1737–1756.

Alexander, L., and J. Handschy, 1998, Fluid flow in a faulted reservoir system: fault trap analysis for the Block 330 field, Eugene Island, south addition, offshore Louisiana; AAPG Bulletin, v. 82, p. 387–411.

Anderson, R., 1993, Recovering dynamic Gulf of Mexico reserves and the U.S. energy future: Oil & Gas Journal, v. 91, no. 17, April 26, p. 85–91.

Anderson, R., P. Flemings, S. Losh, J. Whelan, L. Billeaud, J. Austin, and R. Woodhams, 1994a, The Pathfinder drilling program into a major growth fault in Eugene Island 330, Gulf of Mexico: implications for behavior of hydrocarbon migration pathways:

CD-ROM prepared under Department of Energy contract DE-FC22-93BC14961, 1 CD-ROM.
Anderson, R., P. Flemings, S. Losh, J. Austin, and R. Woodhams, 1994b, Gulf of Mexico growth fault drilled, seen as oil, gas migration pathway: Oil & Gas Journal, v. 92, no. 23, June 6, p. 97–103.
Boles, J., and S. Franks, 1979, Clay diagenesis in Wilcox sandstones of southwest Texas: implications of smectite diagenesis on sandstone cementation: Journal of Sedimentary Petrology, v. 49, p. 55–70.
Chung, M., J. Gormly, and R. Squires, 1988, Origin of gaseous hydrocarbons in subsurface environments: theoretical considerations of carbon isotopic distribution, *in* M. Schoell, ed., Origin of methane in the Earth: Chemical Geology, v. 71, p. 97–103.
Claypool, G., and I. Kaplan, 1974, The origin and distribution of methane in marine sediments: Marine Science, v. 3, p. 99–139.
Curiale, J., and B. Bromley, 1996, Migration induced compositional changes in oils and condensates of a single field: Organic Geochemistry, v. 24, p. 1097–1113.
Finkbeiner, T., M. Zoback, P. Flemings, and B. Stump, 2001, Stress, pore pressure, and dynamically constrained hydrocarbon columns in the South Eugene Island 330 field, northern Gulf of Mexico: AAPG Bulletin, v. 85, p. 1007–1031.
Hanor, J., 1996, Variations in chloride as a driving force in siliciclastic diagenesis, *in* L. Crossey, R. Loucks, and M. Totten, eds., Siliciclastic diagenesis and fluid flow: concepts and applications: SEPM Special Publication 55, p. 3–12.
Harrison, W., and L. Summa, 1991, Paleohydrology of the Gulf of Mexico basin: American Journal of Science, v. 219, p.109–176.
Hart, B., D. Sibley, and P. Flemings, 1997, Seismic stratigraphy, facies architecture, and reservoir character of a Pleistocene shelf-margin delta complex, Eugene Island Block 330 field, offshore Louisiana: AAPG Bulletin, v. 81, p. 380–397.
Hoefs, J., 1981, Isotopic composition of the ocean-atmosphere system in the geologic past, *in* R. O'Connell and W. Fyfe, eds., Evolution of the Earth: American Geophysical Union Geodynamics Series, v. 5, p. 110–119.
Holland, D. S., J. B. Leedy, and D. R. Lammlein, 1990, Eugene Island Block 330 field—U.S.A., offshore Louisiana, *in* E. A. Beaumont and N. H. Foster, eds., Structural traps III: tectonic fold and fault traps: AAPG Treatise of Petroleum Geology, Atlas of Oil and Gas Fields, p. 103–143.
James, A., 1983, Correlation of natural gas by use of carbon isotopic distribution between hydrocarbon components: AAPG Bulletin, v. 67, p. 1176–1191.
Kharaka, Y., and R. Mariner, 1989, Chemical geothermometers and their application to formation waters from sedimentary basins, *in* N. Naeser and T. McCulloch, eds., Thermal history of sedimentary basins: methods and case histories: New York, Springer-Verlag, p. 99–117.
Kissin, Y., 1987, Catagenesis and composition of petroleum: origin of n-alkanes and isoalkanes in petroleum crudes: Geochimica et Cosmochimica Acta, v. 51, p. 2445–2457.
Land, L., and G. MacPherson, 1989, Geochemistry of formation waters, Plio-Pleistocene reservoirs, offshore Louisiana: Transactions of the Gulf Coast Association of Geological Societies, v. 39, p. 421–430.
Land, L., G. MacPherson, and L. Mack, 1988, The geochemistry of saline formation waters, Miocene, offshore Louisiana: Transactions of the Gulf Coast Association of Geological Societies, v. 38, p. 503–511.
Larter, S., and N. Mills, 1991, Phase-controlled molecular fractionations in migrating petroleum charges, *in* W. England and A. Fleet, eds., Petroleum migration: Geological Society Special Publication 59, p. 137–148.
Lin, X., and J. Nunn, 1997, Evidence for Recent migration of geopressured fluids along faults in Eugene Island, Block 330 from estimates of pore water salinity: Transactions of the Gulf Coast Association of Geological Societies, v. 47, p. 419–424.
Losh, S., 1995, Inorganic diagenesis in the SEI Block 330 reservoirs, *in* R. N. Anderson, ed., Quarterly report: U.S. Department of Energy Contract DE-FC22-93BC14961, unpaginated.
Losh, S., 1998, Oil migration in a major growth fault: structural analysis of the Pathfinder core, South Eugene Island Block 330, offshore Louisiana: AAPG Bulletin, v. 82, p. 1694–1710.
Losh, S., L. Eglinton, M. Schoell, and J. Wood, 1999, Vertical and lateral fluid flow related to a large growth fault, South Eugene Island Block 330 field, offshore Louisiana: AAPG Bulletin, v. 83, p. 244–276.
Losh, S., L. Cathles, and P. Meulbroek, 2002, Gas washing of oil along a regional transect, offshore Louisiana: Organic Geochemistry, v. 33, p. 663–665.
MacPherson, G., 1989, Lithium, boron, and barium in formation waters and sediments, northwestern Gulf of Mexico sedimentary basin, Ph.D. thesis, University of Texas at Austin, 286 p.
McBride, B., P. Weimer, and M. Rowan, 1998, The effect of allochthonous salt on the petroleum systems of northern Green Canyon and Ewing Bank (offshore Louisiana), northern Gulf of Mexico: AAPG Bulletin, v. 82, p. 1083–1112.
Meulbroek, P., 1997, Hydrocarbon phase fractionation in sedimentary basins, Ph.D. thesis, Cornell University, Ithaca, New York, 344 p.
Meulbroek, P., L. Cathles, and J. Whelan, 1998, Phase fractionation at South Eugene Island Block 330: Organic Geochemistry, v. 29, p. 223–239.
Milliken, K. L., 1985, Petrology and burial diagenesis of Plio-Pleistocene sediments, northern Gulf of Mexico, Ph.D. thesis, University of Texas at Austin, 112 p.
Moran, J., U. Fehn, and J. Hanor, 1995, Determination of source ages and migration patterns of brines from the U.S. Gulf Coast basin using ^{129}I: Geochimica et Cosmochimica Acta, v. 59, p. 5055–5069.
Peters, K., and J. Moldowan, 1993, The biomarker guide: interpreting molecular fossils in petroleum and ancient sediments: Englewood Cliffs, New Jersey, Prentice Hall, 323 p.
Price, L., L. Wenger, T. Ging, and C. Blount, 1983, Solubility of crude oil in methane gas as a function of pressure and temperature: Organic Geochemistry, v. 4, p. 201–221.
Rice, D., and G. Claypool, 1981, Generation, accumulation, and resource potential of biogenic gas: AAPG Bulletin, v. 65, p. 5–25.
Rowan, M., 1995, Structural styles and evolution of allochthonous salt, central Louisiana outer shelf and upper slope, *in* M. P. A. Jackson, D. Roberts, and S. Snelson, eds., Salt tectonics: a global perspective: AAPG Memoir 65, p. 199–228.
Rowan, M., P. Weimer, and P. Flemings, 1994, Three-dimensional geometry and evolution of a composite, multi-level salt system, western Eugene Island, offshore Louisiana: Transactions of the Gulf Coast Association of Geological Societies, v. 44, p 641–648.
Rowan, M., B. Hart, S. Nelson, P. Flemings, and B. Trudgill, 1998, Three dimensional geometry and evolution of a salt related growth-fault array: Eugene Island 330 field, offshore Louisiana, Gulf of Mexico: Marine and Petroleum Geology, v. 15, p. 309–328.
Schoell, M., and M. Beeunas, 1996, Episodic migration of natural gas: a worldwide phenomenon of dynamic filling of oil and gas fields (abs.): AAPG Annual Convention, Program with Abstracts, v. 5, p. A126.
Schumacher, D., 1993, Eugene Island Block 330 field, offshore Louisiana: geochemical evidence for active hydrocarbon recharging

(abs.): AAPG Annual Convention, Program with Abstracts, p. 179.
Silverman, S., 1965, Migration and segregation of oil and gas, *in* A. Young and G. Galley, eds., Fluids in subsurface environments: AAPG Memoir 4, p. 53–65.
Socki, R. A., H. R. Karlsson, and G. K. Everett Jr., 1992, Extraction technique for the determination of oxygen-18 in water using pre-evacuation glass vials: American Chemical Society, v. 64, p. 829–831.
Thompson, K., 1987, Gas condensate migration and oil fractionation in deltaic systems: Marine and Petroleum Geology, v. 5, p. 237–246.
Thompson, K., M. Kennicutt, and J. Brooks, 1990, Classification of offshore Gulf of Mexico oils and gas condensates: AAPG Bulletin, v. 74, p. 187–198.
Venneman, T. W., and J. R. O'Neil, 1993, A simple and inexpensive method of hydrogen isotope and water analyses of minerals and rocks based on zinc reagent: Chemical Geology, v. 103, p. 227–234.
Whelan, J., 1997, The dynamic migration hypothesis: how fast are oil and gas leaking to the ocean floor and replenishing themselves in some reservoirs?: Sea Technology, v. 38, p. 10–18.
Whelan, J., M. Kennicut, J. Brooks, D. Schumacher, and L. Eglinton, 1994, Organic geochemical indicators of dynamic fluid flow processes in petroleum basins: Organic Geochemistry, v. 22, p. 587–615.